

Effect of Poisson's Ratio on the Elastic Strain Concentration Factor of Notched Bars under Static Tension and under Pure Bending.

H. M. Tlilan

Department of Mechanical Engineering, The Hashemite University, 13115 Zarqa, Jordan

Abstract

As a contribution to the field of strain concentration studies, the coupled influences of Poisson's ratio and the geometric configuration upon the strain concentration factor, defined under triaxial stress state, of notched bars with U-notch, are investigated using the finite element method. Circumferentially U-notched cylindrical bars under tension and rectangular bars with a single edge U-notch under bending with different notch depths are employed here. The results clearly show that the Poisson's ratio has a significant effect on the strain concentration factor, especially for deep and intermediate notch depths. For shallow notches, the elastic strain concentration factor nearly independent of Poisson's ratio. However, for any notch depth the effect of Poisson's ratio becomes prominent with decreasing notch radius. Finally, by fitting the results of FEM analysis, a set of convenient formulas of the elastic strain concentration factor as a function of Poisson's ratio are introduced. These formulas will be useful for any notch depth and radius under the same type of loading employed in the present study.

© 2010 Jordan Journal of Mechanical and Industrial Engineering. All rights reserved

Keywords: Bending; Notched bars; Strain concentration factor; Tension; Poisson's ratio.

Nomenclature

		t_o	Initial notch depth
		ϵ_z	Axial strain
		$(\epsilon_z)_{av}$	Average axial strain
		$(\epsilon_z)_{max}$	Maximum axial strain at the notch root
		ν	Poisson's ratio
		ρ_o	Initial notch radius
		σ_r	Radial stress
		σ_z	Axial stress
		σ_θ	Tangential stress
		$(\sigma_z)_{av}$	Average axial stress at the net section (= P/A)
		$(\sigma_z)_{max}$	Axial stress at the notch root
		$(\sigma_\theta)_{max}$	Tangential stress at the notch root
		F	Transverse load per unit width
A	Current net-section area	$(\epsilon_x)_n$	Nominal strain for pure bending; (Fig. 3)
a	Current distance from the transverse load F to support; (Fig. 1b)	ϵ_x	Longitudinal strain; (Fig. 3)
ao	Initial distance from the transverse load F to support; (Fig. 1b)	$(\epsilon_x^t)_{max}$	Maximum tensile longitudinal strain at the notch root; (Fig. 3)
Do	Initial gross diameter; (Fig. 1a)	σ_x	Longitudinal stress
E	Young's modulus	σ_y	Transverse stress
hc	Current height under compressive $\square x$ at the net section; (Fig. 3)	σ_z	Stress in the width direction
ht	Current height under tensile $\square x$ at the net section; (Fig. 3)	ψ	Distance from the current center of the net section; (Fig. 3)
ho	Initial thickness at the net section; (Fig. 3)	Y	Distance from the current neutral surface; (Fig. 3)
Ho	Initial thickness at the gross section; (Fig. 3)		
$K \square T$	strain-concentration factor under static tension		
$K \square PB$	strain-concentration factor under pure bending		
M	Bending moment per unit width = Fa		
P	Tensile load		
r	Current distance from the center of the net-section ($0 \leq r \leq r_n$)		
r_n	Current net-section radius (= $d/2$)		
s	= r/r_n ($0 \leq s \leq 1.0$)		

* Corresponding author. siva_appisetty1@yahoo.co.in

1. Introduction

Many machines or structural members contain the stress raisers in the form of notches, holes, and fillets. In reality, this kind of stress raisers often the origin of cracks nucleating, growing and easily initiating fracture. The classical solution obtained by researchers has a direct relation with notch geometrical configuration, i.e. notch radius, the notch depth [1, 2]. All these studies results are published and used for engineering design [3]. Almost from the earliest time most of the previous works were based on the stress concentration factor as a tool to predict fracture of machine elements that contains geometrical irregularities [1, 3 – 6]. The stress and conventional strain concentration factors being studied for different types of loading and geometries. It has been concluded that the strain concentration factor is more effective in predicting fracture than the stress concentration factor [7-10]. It should be noted that the conventional strain concentration factor has been defined under uniaxial stress state, while the new strain concentration factor has been defined under triaxial stress state [7,8]. This new definition expresses the concave distribution of the axial strain on the net section from elastic upto general yielding [7-10]. On the other hand, the conventional strain concentration factor failed to express the real irregularities effect as well as the stress concentration factor, especially in plastic deformation. However, the effects of specimen geometry on strain concentration factor have not been completely validated. Tlilan et al. investigated the effect of notch root radius and notch depth on strain concentration factor for circumferential U-notch and single edge U-notch under static tension and pure bending, respectively [8-10].

For three-dimensional problems, i.e. triaxial stress state, the stress and strain concentration factors may change with different material properties such as Poisson's ratio. However, few studied have been done on the effect of material properties on strain concentration factor, especially the new one, which has been defined under triaxial stress state [8-10]. Moreover, few researchers have been considering the mechanical properties effect on stress and strain concentration factors. Since both factors are non-dimensional factors and as it will be shown later, the mechanical property that affects the stress and strain concentration factor is the Poisson's ratio.

Poisson's ratio is defined as the negative of the lateral strain divided by the longitudinal strain. Practically, all ordinary materials, which undergo a lateral contraction when stretched and a lateral expansion when compressed, exhibit a positive Poisson ratio from 0 to 0.5 [11]. The Poisson ratios for various isotropic homogeneous materials are approximately; 0.14-0.16 for SiC, 0.20 for Concrete, 0.21-0.26 for Cast Iron, 0.27-0.3 for steel, 0.42 for Gold, 0.35 for Magnesium, 0.33 Aluminum Alloy, 0.42 for silicon, 0.45 for lead, and nearly 0.5 for rubbers and soft biological tissues [5, 12-15]. Poisson's ratio ν has to be involved in stress and strain concentrations study especially under a three-dimensional or triaxial stress state. The influence of Poisson's ratio on the stress concentration factor varies with the geometric configuration. This is because the stress distributions depend on the change of the element volume and the change of the element volume; depends on Poisson's ratio. For a hyperbolic

circumferential groove in a round bar under tensile load, the stress concentration factors in the axial and circumferential directions are the functions of Poisson's ratio [14]. However, the effect of Poisson's ratio on strain concentration factor has not studied, especially for the newly defined strain concentration factor. Moreover, most of the published works have studied the effect of Poisson's ratio on the conventional strain concentration factor, which has been defined under uniaxial stress state [15].

To this end, the objective of this work is principally to study the effect of Poisson's ratio on the strain concentration factor, defined under triaxial stress state, of notched bars under static tension and pure bending. The influence of Poisson's ratio on the strain concentration factors of circumferential U-notch under tension and single edge U-notch under pure bending have been systematically investigated by use of finite element method (FEM). A set of useful formulae has been obtained with satisfied accuracy by fitting the numerical results.

2. Specimen Geometries and material properties

Two specimens are employed, as shown in Fig.1 ; Cylindrical bar with circumferential U-notch for static tension and rectangular bar with single edge U-notch for pure bending. For static tension, the length of the cylindrical bar is 50.0 mm and the gross diameter D_o is 8.35 mm. Where as, the rectangular bar has length of 160.0 mm, gross thickness H_o of 16.7 mm, and width b_o of 1.0 mm. The computations were performed for under constant gross diameter. While, the notch depth t_o was changed in order to vary the ratio of notch depth to gross diameter (t_o/D_o) and to gross thickness (t_o/H_o) from 0.05 to 0.80. The notch radii employed are 0.5 and 1.0 mm for all cases. To study the effect of Poisson's ratio of the elastic strain concentration factor, Poisson's ratio has been varied from 0.05 to 0.45. Since the analyses is linear elastic, the modulus of elasticity (Young's modulus E) has been chosen to be 200 GPa. This will affect only the displacement and strains but not the stresses. As a result the value of the Young's modulus will not affect the values of the elastic strain concentration factor, because it is a nondimensional factor, which will be shown later in this article.

3. Finite element modeling

The FE method with the eight-node isoparametric quadrilateral element was used in the context of triaxial stress state isotropic elasticity for all the computations. Because of the symmetry of the bar, one-quarter of the specimen is modeled for static tension, whereas one half of the specimen is modeled for pure bending, as shown in Fig.2. The boundary conditions for every model used in the calculations are indicated in the same Figure. A uniform tensile load was applied to the end of the unnotched part of the bar for static tension. For pure bending, a transverse load F of 1 N/mm was applied at 45 mm from the net section, which is enough to obtain the notch effect.

The accuracy of the finite element analysis models was checked by monitoring the strain distribution on the net section. There are a total of 540 elements and 1667 nodes

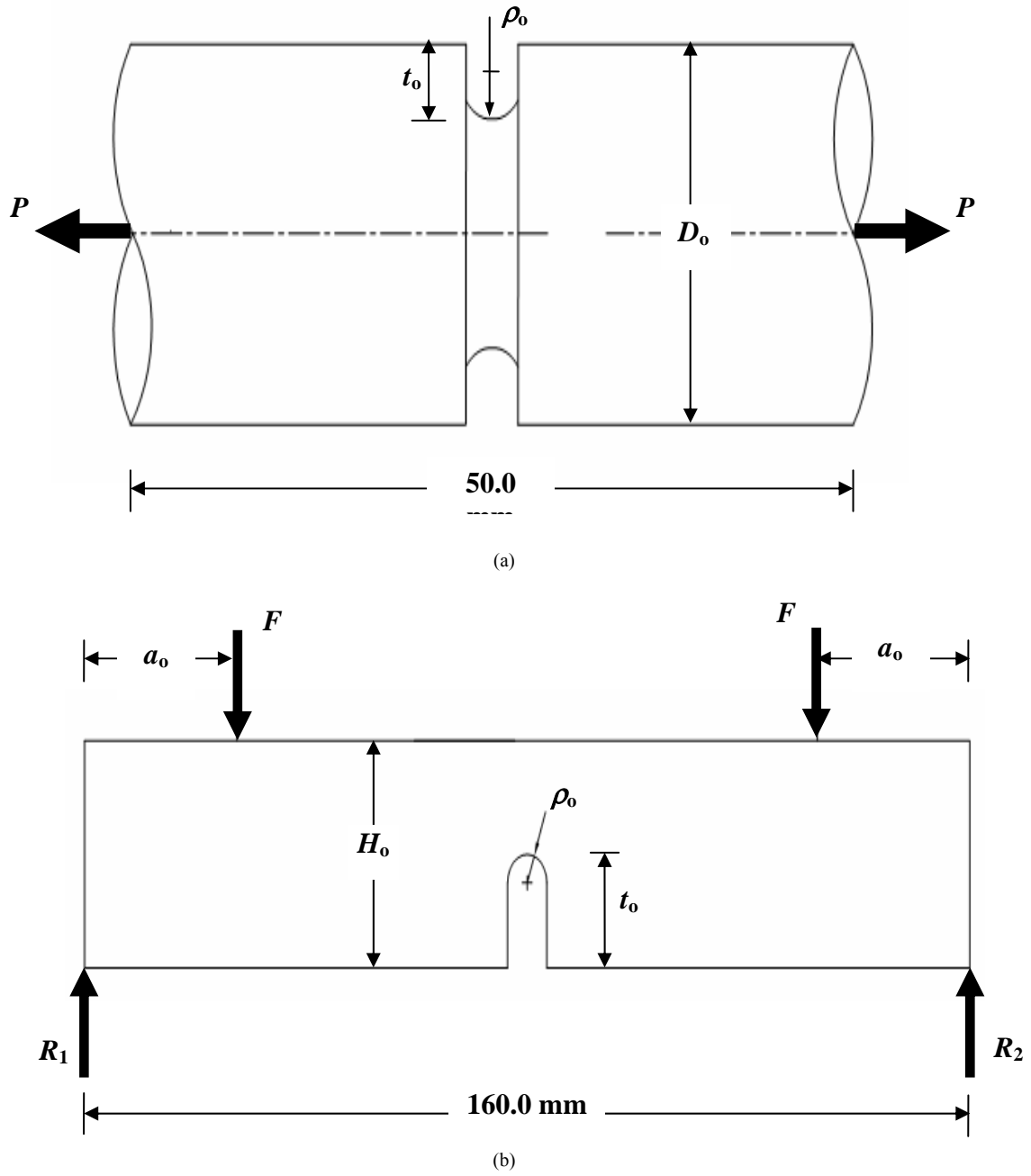


Figure 1. Geometrical properties of the employed specimens: (a) static tension; (b) pure bending.

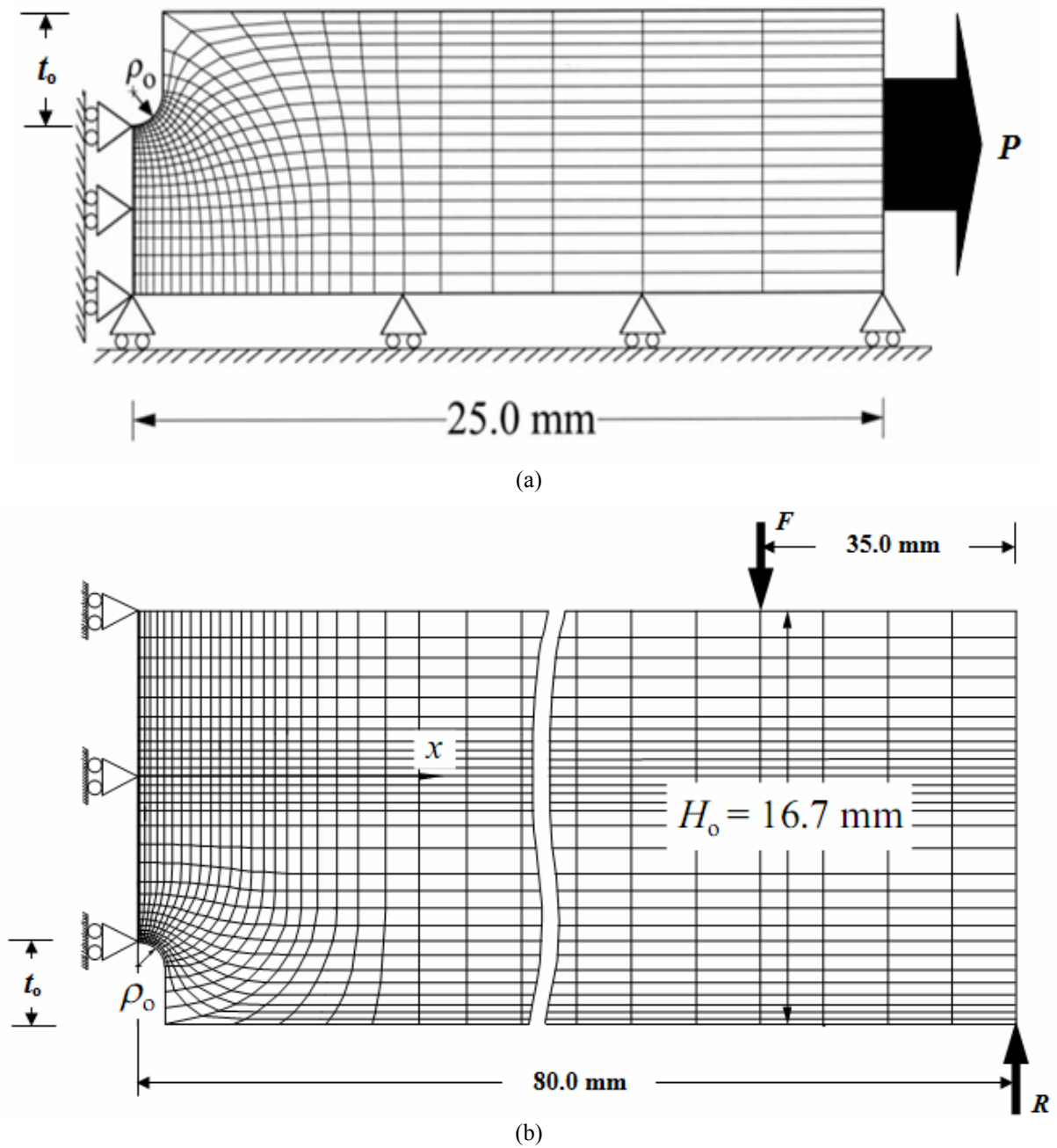


Figure 2. FEM model of the employed specimens: (a) static tension; (b) pure bending.

in the model for static tension, where as 1560 elements and 4845 nodes for pure bending. It should be noted that calculations for pure bending problem have been done under the plane strain condition [9].

4. Relation between strain concentration factor and Poisson’s ratio

4.1. Static tension

The strain concentration factor K_{ϵ}^T employed here has been recently defined under triaxial stress states (Majima, 1999; Tlilan et.al., 2005). This definition gives good consistent results with the axial strain distribution upto general yielding, while the conventional definition showed inconsistency with axial strain distribution on the net section, as it had been defined under uniaxial stress state [8]. The strain concentration factor is defined as follows:

$$K_{\epsilon}^T = \frac{(\epsilon_z)_{max}}{(\epsilon_z)_{av}} \tag{1}$$

where; $(\epsilon_z)_{max}$ is the maximum axial strain; i.e. the axial strain at the notch root. $(\epsilon_z)_{av}$ is the average or nominal axial strain on the net section. The average or nominal axial strain has been defined under triaxial stress state.

$$\begin{aligned} (\epsilon_z)_{av} &= \frac{1}{A} \int_A \epsilon_z(r) dA \\ &= \frac{1}{\pi r_n^2} \int_0^{r_n} \epsilon_z(r) 2\pi r dr \end{aligned} \tag{2}$$

In elastic deformation and using Hook’s law the axial strain is transformed to be

$$\epsilon_z = \frac{1}{E} [\sigma_z - \nu(\sigma_{\theta} + \sigma_r)] \tag{3}$$

Moreover, the axial strain at the notch root; i.e. the maximum axial strain, becomes

$$\begin{aligned} (\epsilon_z)_{max} &= \frac{1}{E} \{(\sigma_z)_{notch\ root} - \nu[(\sigma_{\theta})_{notch\ root} + (\sigma_r)_n]\} \\ &= \frac{1}{E} \{(\sigma_z)_{max} - \nu[(\sigma_{\theta})_{max} + (\sigma_r)_{max}]\} \end{aligned} \tag{4}$$

Substitute Eq.(3) into Eq.(2) leads to the elastic nominal or average axial strain

$$\begin{aligned} (\epsilon_z)_{av} &= \frac{1}{\pi r_n^2} \int_0^{r_n} \left[\frac{\sigma_z}{E} - \frac{\nu}{E} (\sigma_{\theta} + \sigma_r) \right] 2\pi r dr \\ &= \frac{1}{E} \left\{ (\sigma_z)_{av} - \frac{\nu}{\pi r_n^2} \int_0^{r_n} (\sigma_{\theta} + \sigma_r) 2\pi r dr \right\} \end{aligned} \tag{5}$$

Substitute Eqs. (4) and (5) into Eq.(1) gives

$$\begin{aligned} K_{\epsilon}^T &= \frac{\frac{1}{E} \{(\sigma_z)_{max} - \nu[(\sigma_{\theta})_{max} + (\sigma_r)_{max}]\}}{\frac{1}{E} \left\{ (\sigma_z)_{av} - \frac{\nu}{\pi r_n^2} \int_0^{r_n} (\sigma_{\theta} + \sigma_r) 2\pi r dr \right\}} \\ &= \frac{(\sigma_z)_{max} - \nu[(\sigma_{\theta})_{max} + (\sigma_r)_{max}]}{(\sigma_z)_{av} - \frac{\nu}{\pi r_n^2} \int_0^{r_n} (\sigma_{\theta} + \sigma_r) 2\pi r dr} \end{aligned} \tag{6}$$

It is clear from Eq.(6) that Poisson’s ratio is the only factor which affects the elastic strain concentration factor in addition to local stress values at the notch root and the stress distribution on the net section. It should be noted that the conventional strain concentration factor neglect Poisson’s ratio effect. This is due to the definition of the conventional strain concentration factor under uniaxial stress state [8].

4.2. Pure bending

For pure bending, the strain concentration factor K_{ϵ}^{PB} has been defined as the ratio of the maximum longitudinal strain at the notch root $(\epsilon_x^t)_{max}$ to the nominal longitudinal strain on the net section $(\epsilon_x)_n$ [9];

$$K_{\epsilon}^{PB} = \frac{(\epsilon_x^t)_{max}}{(\epsilon_x)_n} \tag{7}$$

This strain concentration factor has been introduced by defining the nominal longitudinal strain under triaxial state in elastic deformation as well as plastic deformation. The new nominal longitudinal strain considered the effect of transverse stress, which it was neglected in the conventional definition. The new nominal longitudinal strain is defined as [9];

$$(\epsilon_x)_n = \frac{6}{(h_t + h_c)^2} \int_{-h_c}^{h_t} \epsilon_x Y dY \tag{8}$$

Where; h_t is the current height from the neutral surface to the notch root and h_c is the current height from the neutral surface to the unnotched surface opposite to the notch root, as shown in Fig. 3. In elastic deformation; $h_t + h_c \approx h_o$, the new nominal longitudinal strain is

$$(\epsilon_x)_n = \frac{6}{E h_o^2} \int_{-h_c}^{h_t} [\sigma_x - \nu(\sigma_y + \sigma_z)] Y dY \tag{9}$$

Under plane strain condition and using Hooke's law; $(\sigma_z)_{nr} = \nu[(\sigma_x)_{nr} + (\sigma_y)_{nr}]$, the new nominal longitudinal strain can be rewritten as

$$\begin{aligned} (\varepsilon_x)_n &= \frac{6}{E h_o^2} \left[(1-\nu^2) \int_{-h_c}^{h_t} \sigma_x Y dY - \nu(1+\nu) \int_{-h_c}^{h_t} \sigma_y Y dY \right] \\ &= \frac{6}{E h_o^2} \left[(1-\nu^2)M - \nu(1+\nu) \int_{-h_c}^{h_t} \sigma_y Y dY \right] \end{aligned} \quad (10)$$

Moreover, the maximum longitudinal strain can be written as

$$(\varepsilon_x^t)_{max} = \frac{1}{E} \left\{ (\sigma_x^t)_{nr} - \nu[(\sigma_y)_{nr} + (\sigma_z)_{nr}] \right\} \quad (11)$$

which transformed to following form under plane strain condition

$$\begin{aligned} (\varepsilon_x^t)_{max} &= \frac{1}{E} \left\{ (\sigma_x^t)_{nr} - \nu[(\sigma_y)_{nr} + \nu(\sigma_x)_{nr} + \nu(\sigma_y^t)_{nr}] \right\} \\ &= \frac{1}{E} \left[(1-\nu^2)(\sigma_x^t)_{nr} - (\nu+\nu^2)(\sigma_y)_{nr} \right] \end{aligned} \quad (12)$$

However, at the notch root the transverse stress is equal to zero; i.e. $(\sigma_y)_{nr} = 0.0$ (Tilhan et al., 2006), therefore

$$(\varepsilon_x^t)_{max} = \frac{(1-\nu^2)}{E} (\sigma_x^t)_{nr} = \frac{(1-\nu^2)}{E} (\sigma_x^t)_{max} \quad (13)$$

Substitution of Eq.(10) and Eq.(13) into Eq. (7) leads to

$$\begin{aligned} K_\varepsilon^{PB} &= \frac{\frac{(1-\nu^2)}{E} (\sigma_x^t)_{max}}{\frac{6}{E h_o^2} \left[(1-\nu^2)M - \nu(1+\nu) \int_{-h_c}^{h_t} \sigma_y Y dY \right]} \\ &= \frac{(1-\nu^2)h_o^2 (\sigma_x^t)_{max}}{6 \left[(1-\nu^2)M - (\nu+\nu^2) \int_{-h_c}^{h_t} \sigma_y Y dY \right]} \end{aligned} \quad (14)$$

Rearranging the previous equation gives the elastic strain concentration factor for pure bending

$$K_\varepsilon^{PB} = \frac{h_o^2 (\sigma_x^t)_{max}}{6M - \frac{6(\nu+\nu^2)}{(1-\nu^2)} \int_{-h_c}^{h_t} \sigma_y Y dY} \quad (15)$$

It has shown that

$$\int_{-h_c}^{h_t} \sigma_y Y dY \neq 0.0$$

This indicates that Eq. (15) clearly showed the effect of Poisson's ratio on the elastic strain concentration factor. This effect can not be shown by the conventional definition, which is essentially attributed to the definition

of the strain concentration factor under uniaxial stress state (Tilhan et al., 2006).

5. Results and discussion

5.1. Static tension

The effect of varying Poisson's ratio on the elastic K_ε^T for the employed notched bars is shown in Figs. 4, respectively. In each of these figures, the elastic K_ε^T are presented for nine different values of Poisson's ratio, i.e. $\nu = 0.05, 0.1, 0.15, 0.20, 0.25, 0.30, 0.35, 0.40$ and 0.45 . The variations of K_ε^T with the ratio of notch depth to gross diameter (t_o/D_o) are shown in Fig. 4. It is shown that the variation of the strain concentration factor depends on Poisson's ratio for all notched bars employed. This is prominent in the range $0.20 < t_o/D_o \leq 0.80$, as shown in Fig. 4. Actually, the elastic K_ε^T increases with increasing Poisson's ratio for notches with $0.20 < t_o/D_o \leq 0.80$ and the intermediate notch depth has the maximum elastic K_ε^T for all Poisson's ratio values and notch radii employed.

In the former set of figures, Poisson's ratio influences the elastic K_ε^T curve only on its magnitude. As a result, the variation in the elastic K_ε^T with Poisson's ratio is not clear, especially for deep and shallow notches. In order to clarify the effect of the Poisson's ratio, the elastic K_ε^T is plotted in figures 5 - 15 as a function of Poisson's ratio ν for each of the notch depths and radii values used in the investigation. For the same notch depth, there appears to be a trend towards increasing K_ε^T with an increase in ν or $0.20 < t_o/D_o \leq 0.80$. Further, the trend appears to be greater for the all notch depths at $\rho = 0.5$ mm than for those at $\rho = 1.0$ mm. However, the elastic K_ε^T becomes nearly constant or slightly decreases with increasing ν for the shallow notches ($0.05 < t_o/D_o \leq 0.15$).

Generally, it is believed that if notch depth is constant the effect of Poisson's ratio is not very large. In the above mentioned results, it is found that for deep and intermediate notch depths under tension the effect of Poisson's ratio can not be negligible. However, for shallow notches under tension, the effect of ν is not very large. Therefore, the effect of a negative Poisson's ratio can effectively enhance the deformation capability in the deformation of materials, which is vital to the fracture mechanics of a lot of machine elements, especially when it contains irregularities.

In the finite element results mentioned above and by curve fitting; a convenient 7th order polynomial formula can be proposed. As a results, Tables 1 and 2 give the polynomials that are obtained for elastic K_ε^T as a function of ν .

5.2. Pure bending

The elastic strain concentration factor under bending (K_ε^{PB}) variations with notch depth (t_o/H_o) for different Poisson's ratios are shown in Fig. 16. It is obvious that the general trend of the variation of K_ε^{PB} with t_o/H_o is independent of Poisson's ratio. Actually, the elastic K_ε^{PB} increases with increasing t_o/H_o and reaches maximum value at $t_o/H_o = 0.2$ for Poisson's ratio of 0.45. On the other hand, the maximum elastic K_ε^{PB} occurs at $t_o/H_o = 0.25$ for Poisson's ratio values less than 0.45. The Poisson's ratio effect is prominent in the range where 0.05

$< t_o / H_o \leq 0.5$. This means that the elastic K_e^{PB} is nearly independent of Poisson's ratio for deep notches, i.e. $t_o / H_o > 0.5$. The smaller the notch radius is, the larger the effect of Poisson's ratio on strain concentration factor is.

Figures 17 - 26 show the relationship between the elastic K_e^{PB} and Poisson's ratio (ν). As it can be seen, figures 17 - 26 show the dependence of the elastic K_e^{PB} on Poisson's ratio values. For notches with $0.2 < t_o / H_o \leq 0.8$, the elastic K_e^{PB} gradually increases with increasing ν and reaches maximum values at $\nu \approx 0.3$. After that, the elastic K_e^{PB} shows a slight decrease with increasing ν . On the other hand, the elastic K_e^{PB} increases with increase in ν for the shallow notches, i.e. $t_o / H_o = 0.05, 0.1, \text{ and } 0.15$. This trend is independent of notch radius. However, for the same notch depth and Poisson's ratio, as it can be seen in figures 17 - 26; the elastic K_e^{PB} increases with decreasing notch radius.

Tables 3 and 4 gives an empirical expression for the elastic K_e^{PB} as a function of ν , which is obtained by fitting the FEM results for all notch depths and radii employed. Therefore, the empirical expression can be used conveniently in elastic K_e^{PB} prediction of single edged U-notched bars with various notch geometries and different valued of ν .

6. Conclusions

By using three-dimensional FEM analysis, the effect of Poisson's ratio on the elastic strain concentration factor, defined under triaxial stress state, of a notched bars for different specimen sizes and different loading types have been evaluated. Taking the advantage of a recent formulation of the strain concentration factor under triaxial stress state, which is suitable for expressing the actual strain and stress distributions in the vicinity of notches in machine elements. On the other hand, the conventional strain concentration factor has been defined under uniaxial stress state, which neglects or can not predict the actual effect of the Poisson's ratio on the strain concentration. The shown results in this work lead to the conclusion that Poisson's ratio has a significant effect on the elastic strain concentration factor for the geometries and, treated loading types. According to the present study the following conclusions are drawn:

1. It is established in this work that for axially loaded members and for the selected geometry treated, the values of the elastic strain concentration factor appreciably increases with increasing Poisson's ratio for notches with $0.20 < t_o / D_o \leq 0.80$. However, the elastic strain concentration factor is nearly constant or slightly decreasing with the increase in the Poisson's ratio for shallow notches, i.e. $0.05 < t_o / D_o \leq 0.15$.
2. For pure bending, the elastic strain concentration factor increases and attains a maximum value, then it decreases as the values of Poisson's ratio increase for notches with $0.2 < t_o / H_o \leq 0.8$. On the other hand, the

elastic strain concentration factor slightly increases with increasing Poisson's ratio values for $t_o / H_o = 0.05, 0.1, \text{ and } 0.15$.

3. For all loading types and notch geometries employed, the effect of Poisson's ratio on the elastic strain concentration factor is more pronounced in extremely deep and intermediate notch depths than that for shallow notches.

References

- [1] M.M. Leven, M.M. Frocht, "Stress-concentration factors for single notch in flat bar in pure and central bending". J. Appl. Mechanics, Vol. 74, 560-56; 1952.
- [2] H. Neuber, "Theory of stress concentration factor for shear-strained prismatical bodies with arbitrary nonlinear stress-strain law". J. Appl. Mechanics, Vol. 28, 544-550; 1961.
- [3] W.D. Pilkey, Peterson's Stress Concentration Factors. Wiley, New York; 1997.
- [4] K. Nishida, Stress Concentration (in Japanese). Morikita Shuppan, Tokyo; 1974.
- [5] A. Kato, "Design equation for stress concentration factors of notched strips and grooved shafts". J. strain analysis, Vol 26, 21-28; 1991.
- [6] N.-A. Noda, M. Sera, Y. Takase, "Stress concentration factors for round and flat test specimens with notches". Int. J. Fatigue, Vol. 17, No. 3, 163-178; 1995,
- [7] T. Majima, "Strain-concentration factor of circumferentially notched cylindrical bars under static tension". J. Strain Analysis, Vol. 34, No. 5, 347-360; 1999.
- [8] H.M. Tlilan, S. Yousuke, T. Majima, "Effect of notch depth on strain-concentration factor of notched cylindrical bars under static tension". European Journal of Mechanics A / Solids, Vol. 24, No. 3, 406-416; 2005.
- [9] H.M. Tlilan, N. Sakai, T. Majima, "Effect of notch depth on strain-concentration factor of rectangular bars with a single-edge notch under pure bending". Int. J. Solids and Structures, Vol. 43, 459-474; 2006.
- [10] H.M. Tlilan, A.S. Al-Shyyab, A.M. Jawarneh, A.K. Ababneh, "strain-concentration factor of circumferentially v-notched cylindrical bars under static tension". Journal of Mechanics, Vol. 24, No. 4, 419-428; 2008.
- [11] W.D. Pilkey, Formulas for stress, strain, and structural matrices. 2nd ed., John Wiley & Sons, New York; 2005.
- [12] H. Neuber, Theory of notch stresses: principles for exact calculation of strength with reference to structural form and material. 2nd ed., Springer Verlag, Berlin; 1958.
- [13] J. Dundurs, "Dependence of stress on Poisson's ratio in plane elasticity". Int J Solids Struct. Vol. 3, 1013-1021; 1967.
- [14] R.J. Grant, M. Lorenzo, J. Smart, "The effect of Poisson's ratio on stress concentrations". J Strain Anal Engng., Vol. 42, 95-104; 2007.
- [15] Y. Zheng, "Stress and strain concentration factors for tension bars of circular cross-section with semicircular groove". Engineering Fracture Mechanics., Vol. 76, 1683-1690; 2009.

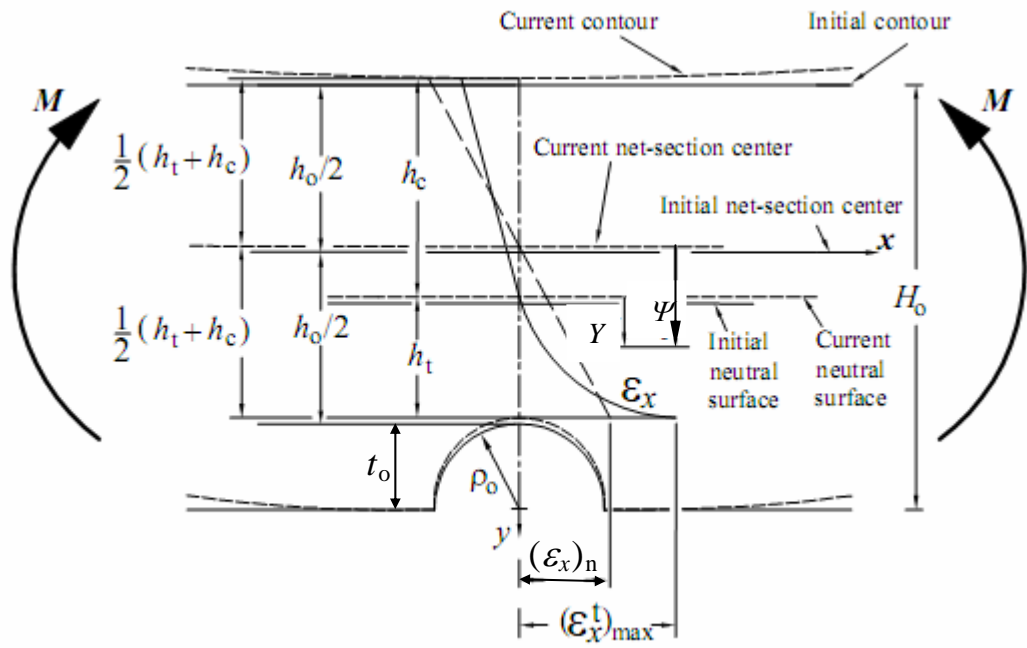
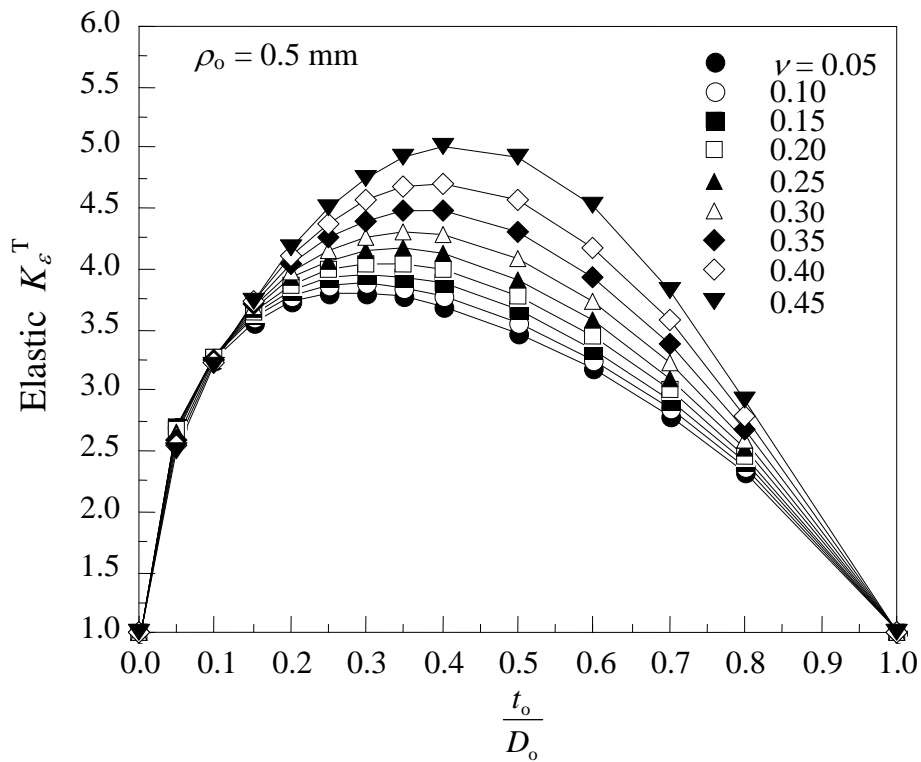
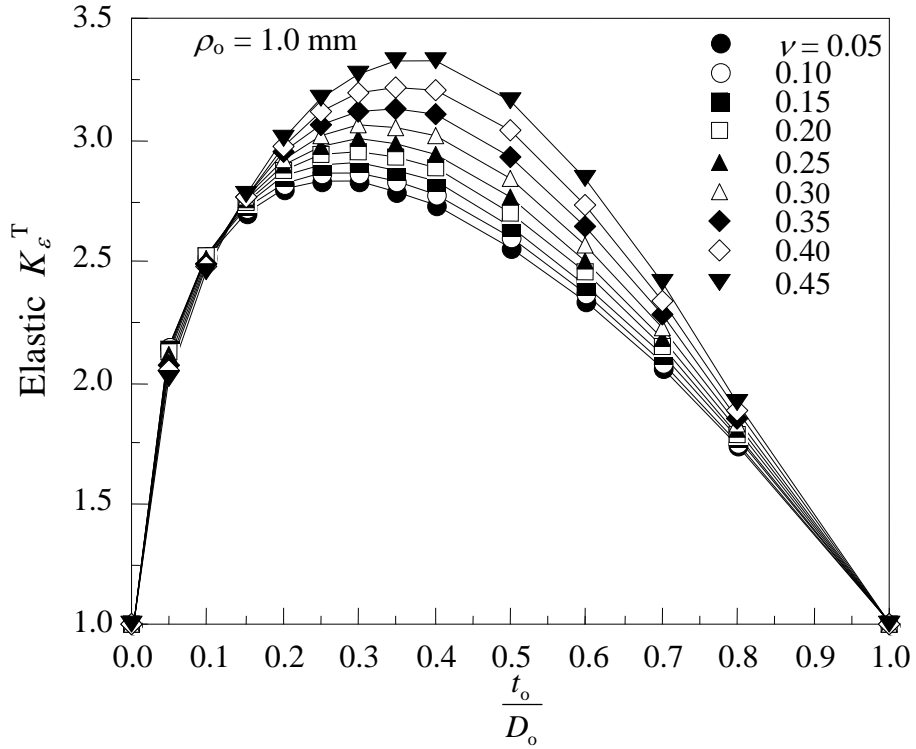


Figure 3. Initial and current contours for pure bending.



(a)



(b)

Figure 4. Effect of Poisson's ratio on the variation of elastic K_ϵ^T with notch depth: (a) $\rho_o = 0.5 \text{ mm}$; (b) $\rho_o = 1.0 \text{ mm}$.

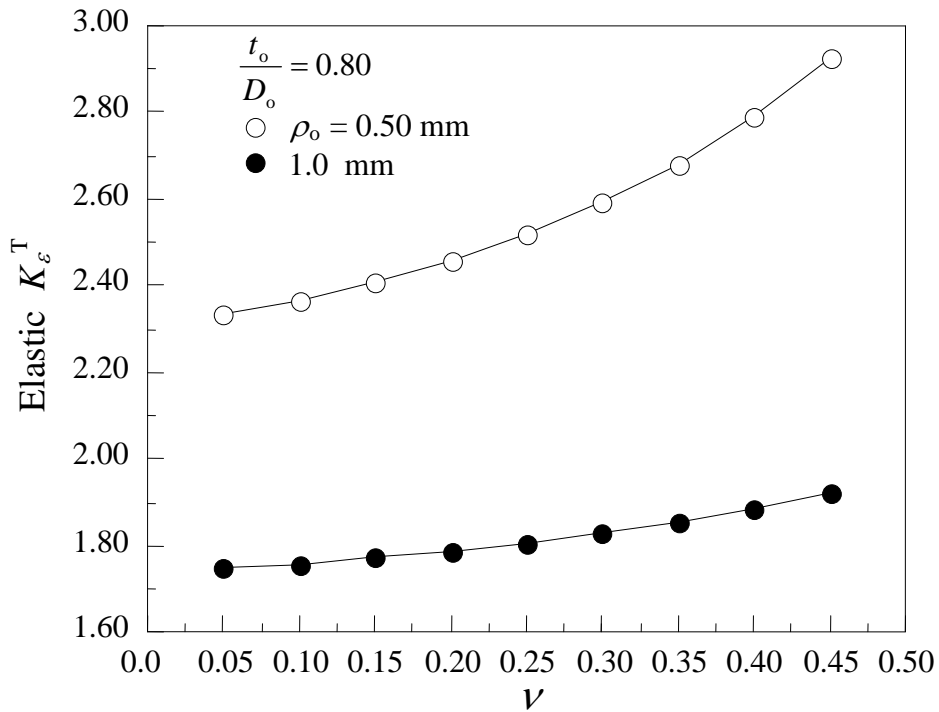


Figure 5. Variation of the elastic K_ϵ^T with Poisson's ratio for $t_o/D_o = 0.80$

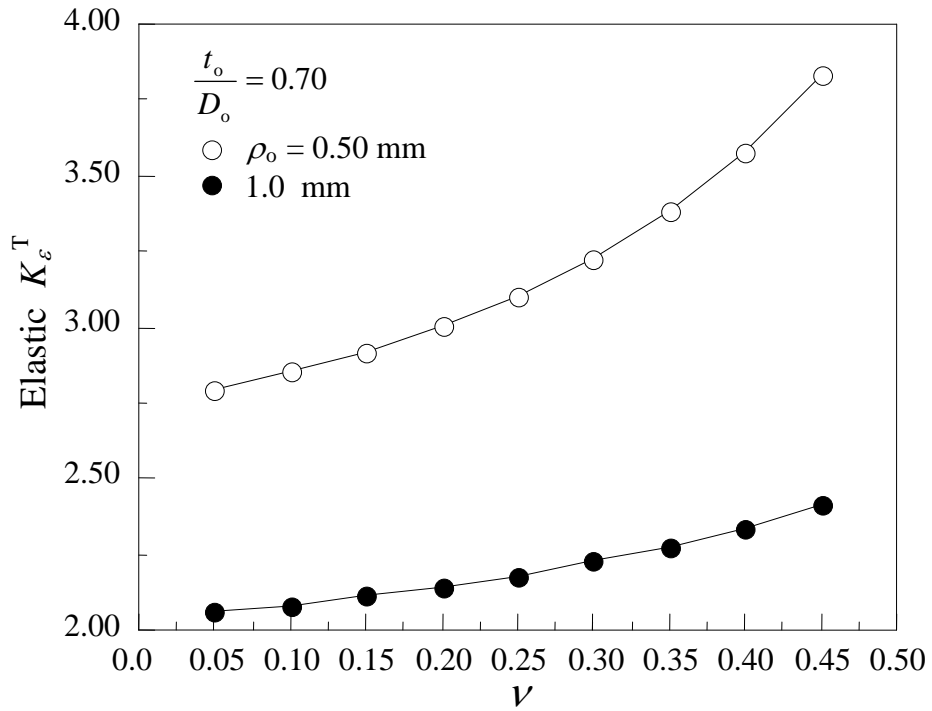


Figure 6. Variation of the elastic K_e^T with Poisson's ratio for $t_o/D_o = 0.70$

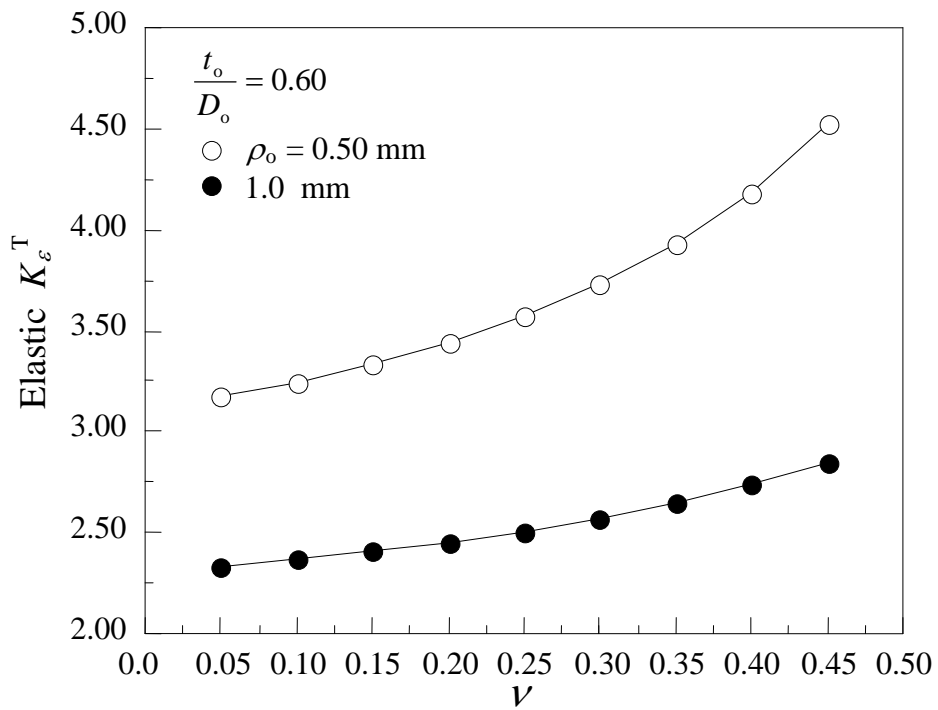


Figure 7. Variation of the elastic K_e^T with Poisson's ratio for $t_o/D_o = 0.60$

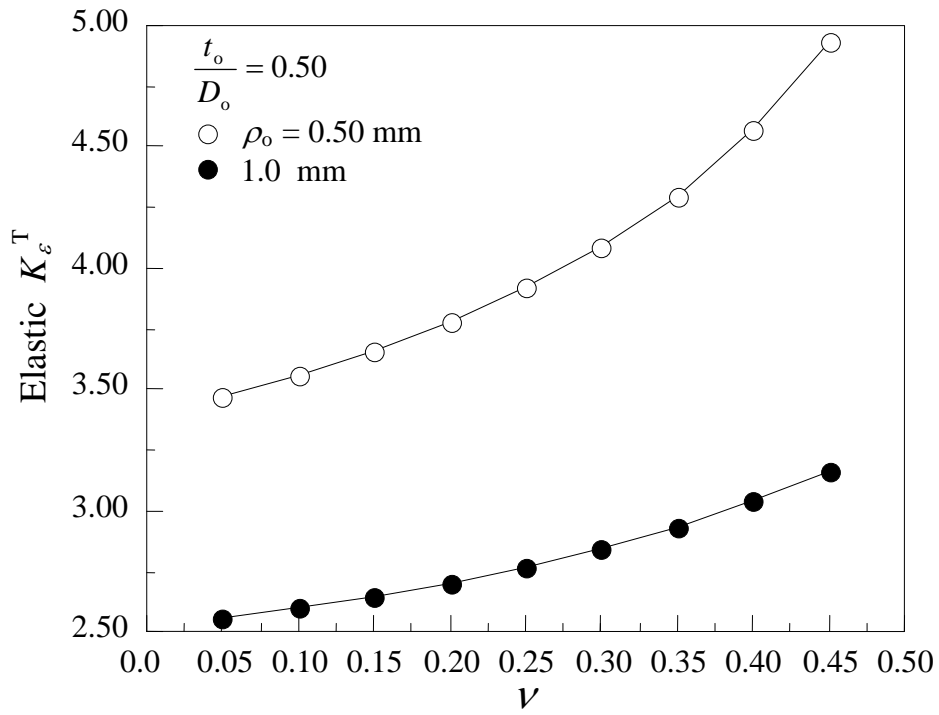


Figure 8. Variation of the elastic K_ϵ^T with Poisson's ratio for $t_o/D_o = 0.50$

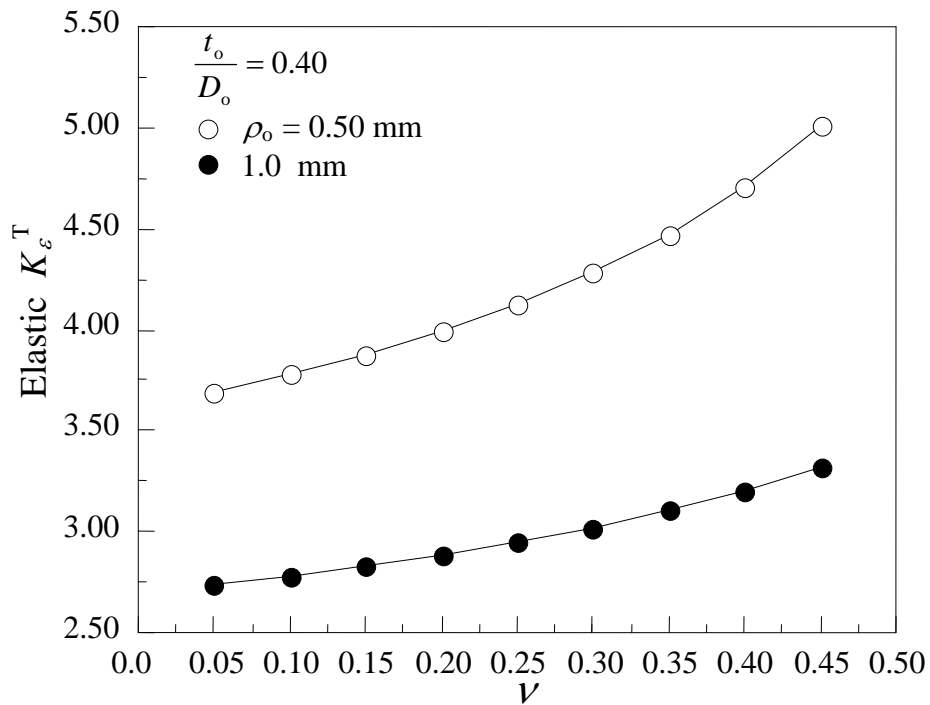


Figure 9. Variation of the elastic K_ϵ^T with Poisson's ratio for $t_o/D_o = 0.40$

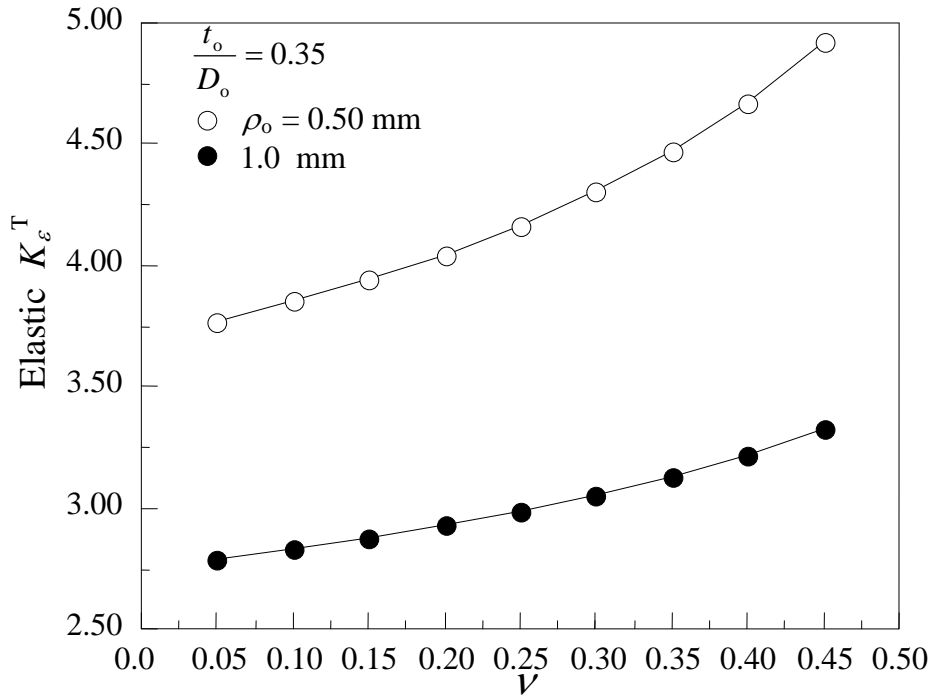


Figure 10. Variation of the elastic K_ϵ^T with Poisson's ratio for $t_o/D_o = 0.35$

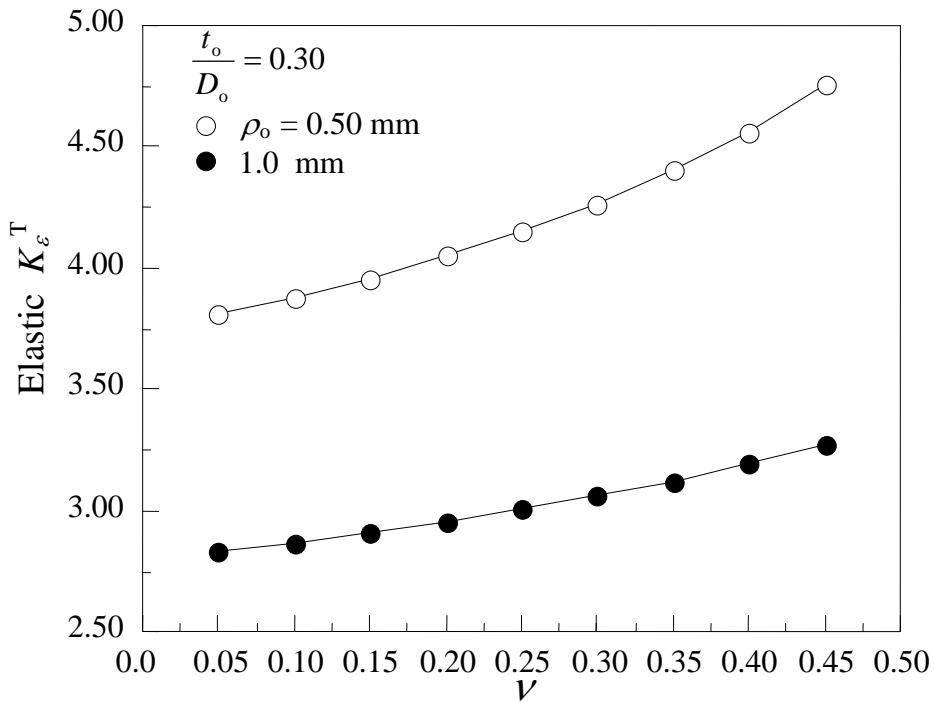


Figure 11. Variation of the elastic K_ϵ^T with Poisson's ratio for $t_o/D_o = 0.30$

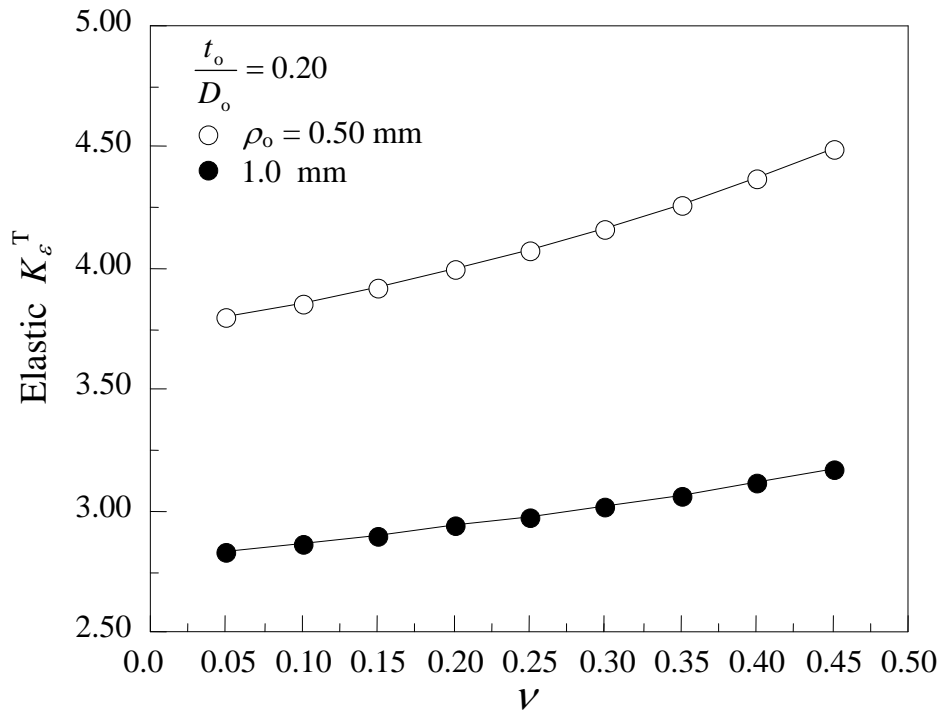


Figure 12. Variation of the elastic K_ϵ^T with Poisson's ratio for $t_o/D_o = 0.20$

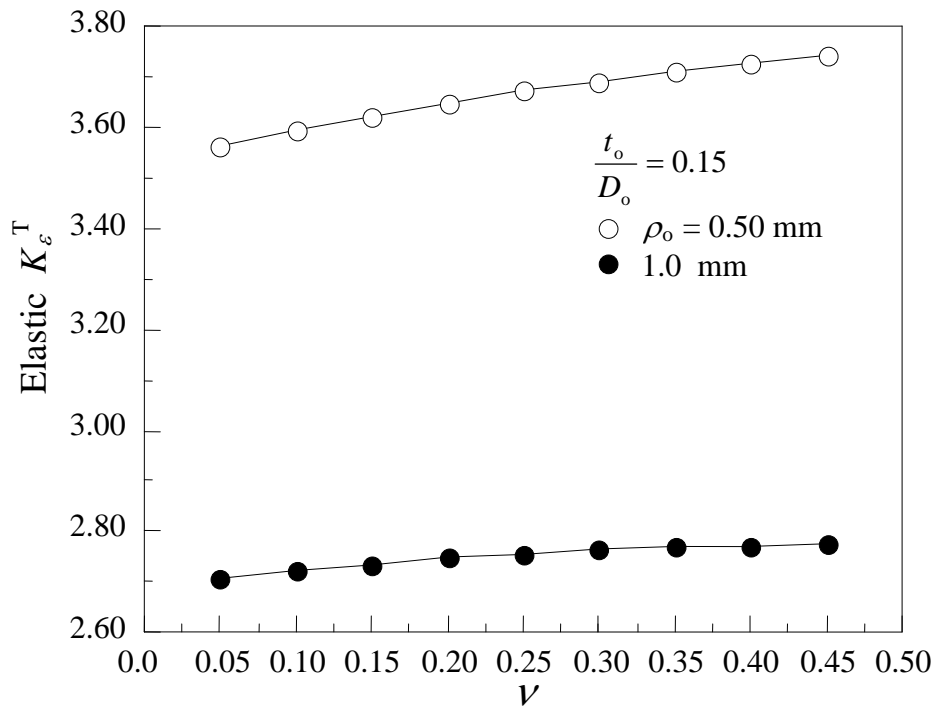


Figure 13. Variation of the elastic K_ϵ^T with Poisson's ratio for $t_o/D_o = 0.15$

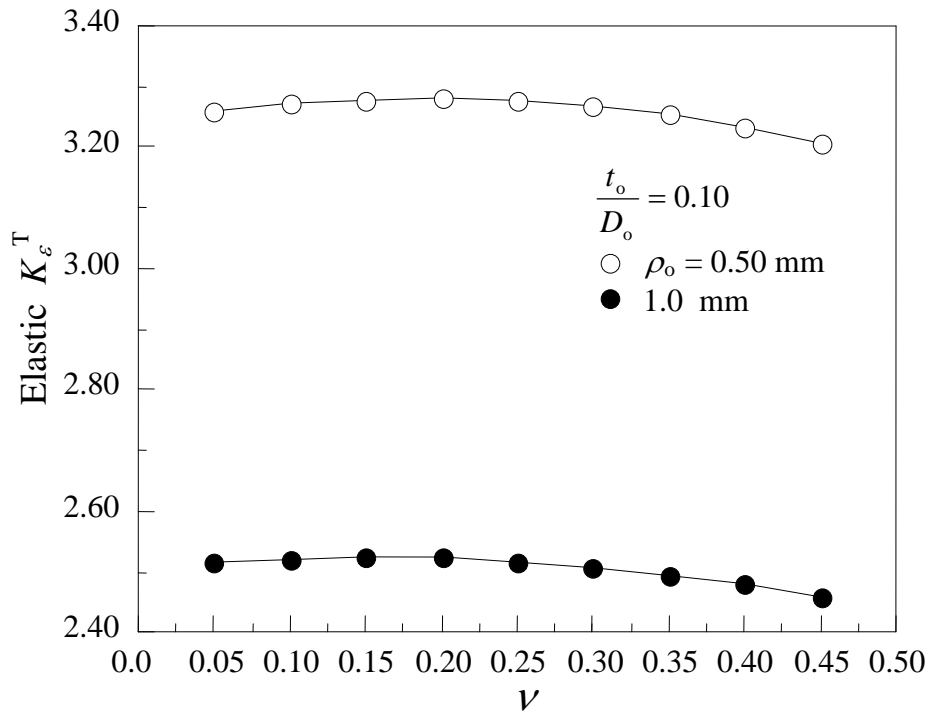


Figure 14. Variation of the elastic K_ϵ^T with Poisson's ratio for $t_o/D_o = 0.10$

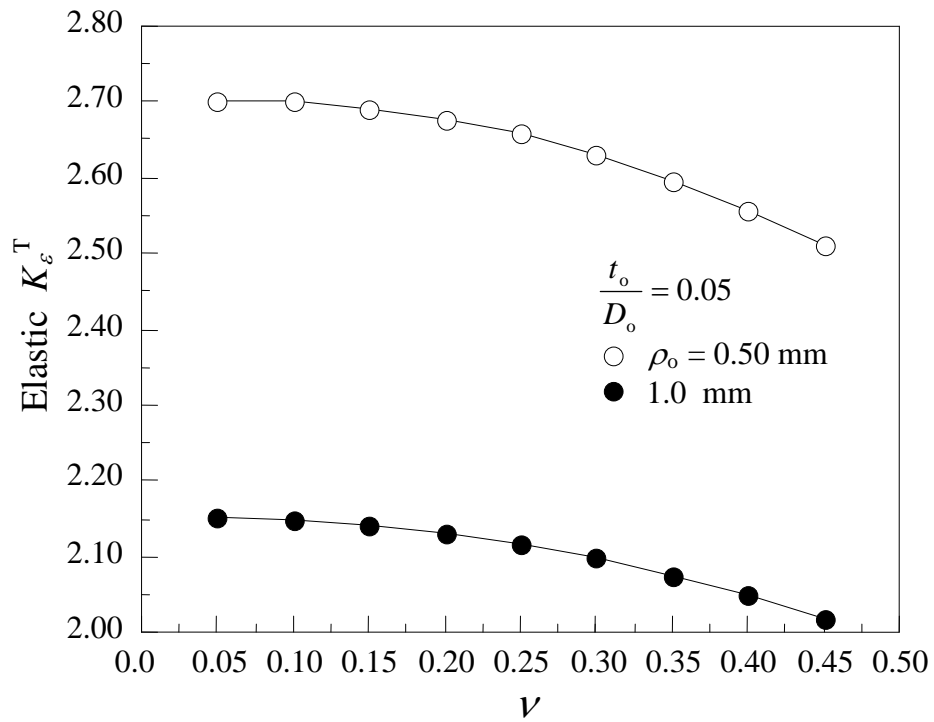
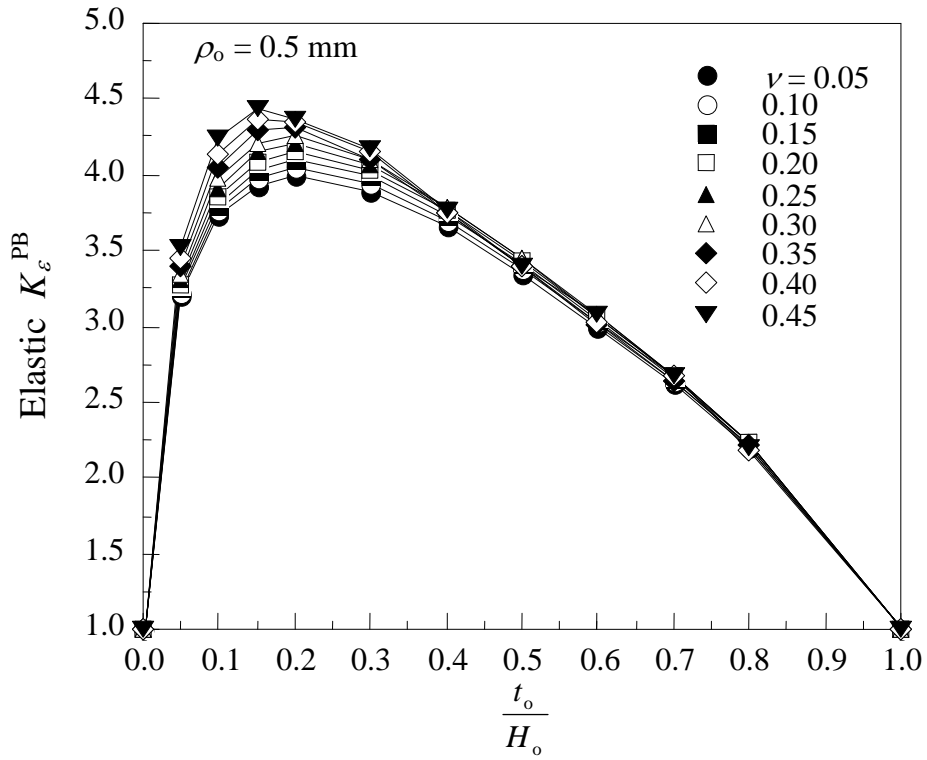
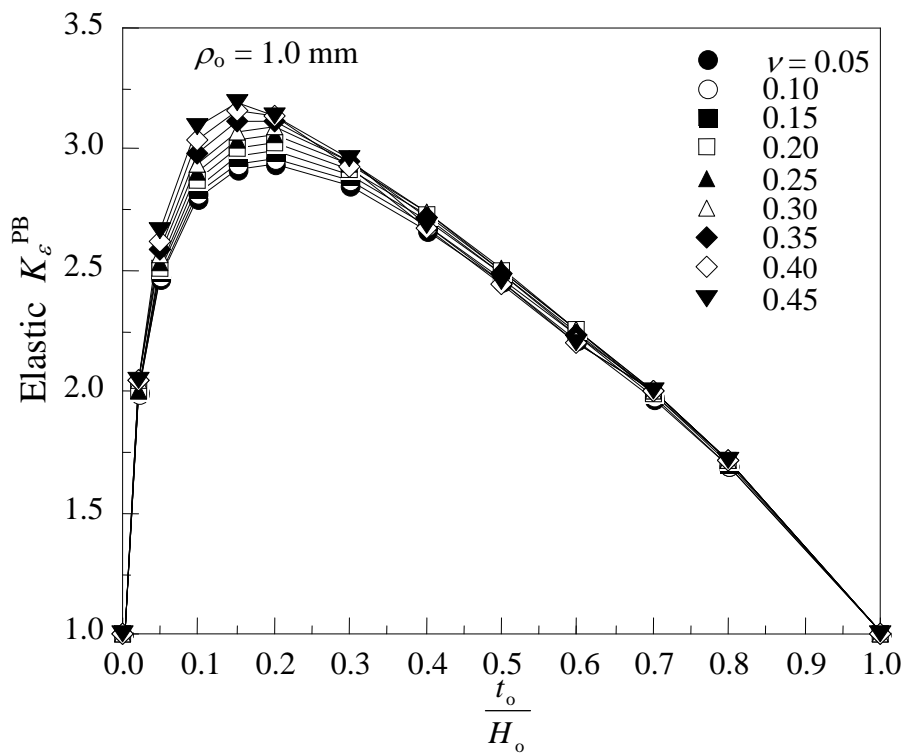


Figure 15. Variation of the elastic K_ϵ^T with Poisson's ratio for $t_o/D_o = 0.05$



(a)



(b)

Figure 16. Effect of Poisson's ratio on the variation of elastic K_ϵ^{PB} with notch depth: (a) $\rho_o = 0.5 \text{ mm}$; (b) $\rho_o = 1.0 \text{ mm}$.

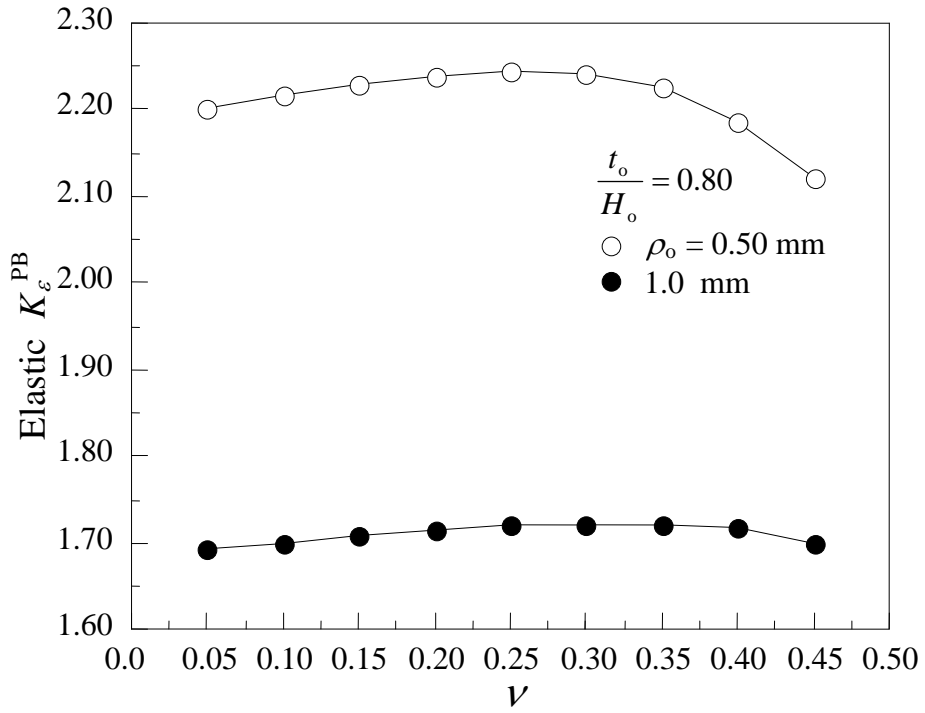


Figure 17. Variation of the elastic K_ϵ^{PB} with Poisson's ratio for $t_o/H_o = 0.80$

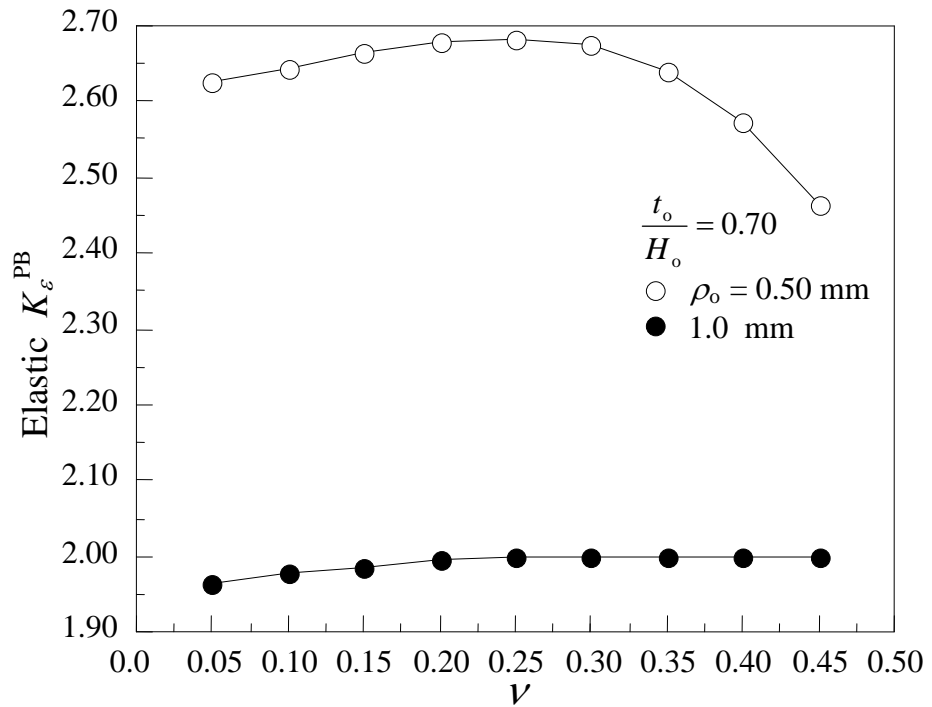


Figure 18. Variation of the elastic K_ϵ^{PB} with Poisson's ratio for $t_o/H_o = 0.70$

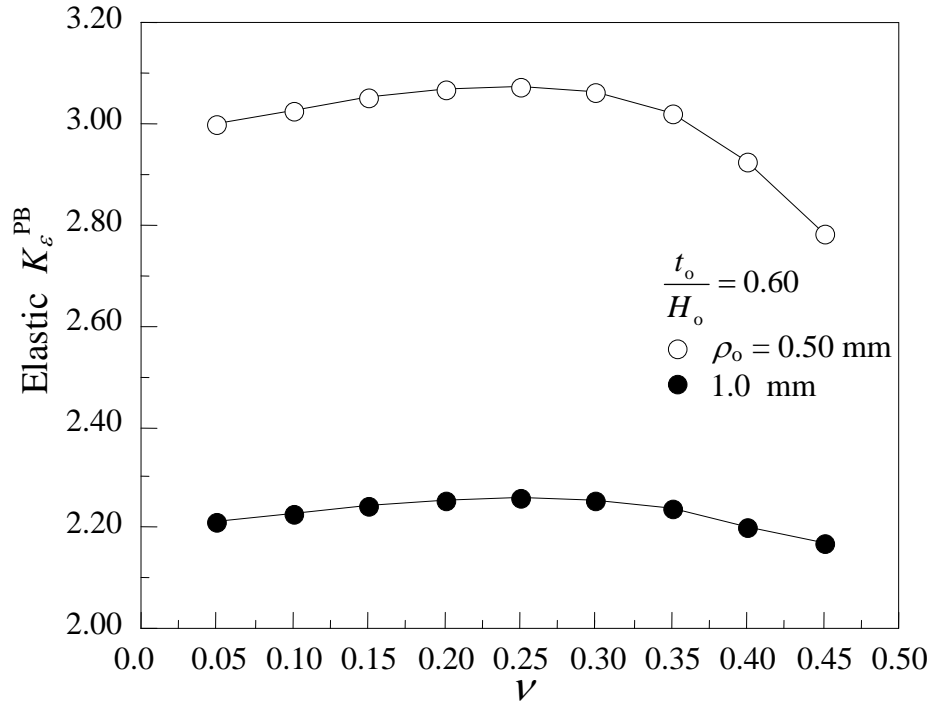


Figure 19. Variation of the elastic K_ϵ^{PB} with Poisson's ratio for $t_o/H_o = 0.60$

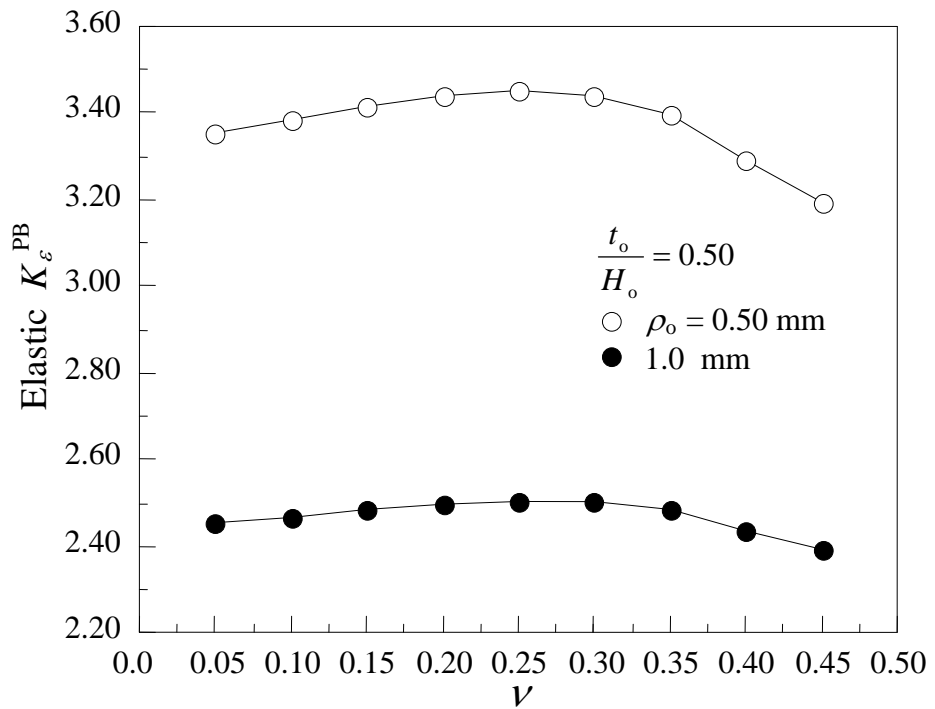


Figure 20. Variation of the elastic K_ϵ^{PB} with Poisson's ratio for $t_o/H_o = 0.50$

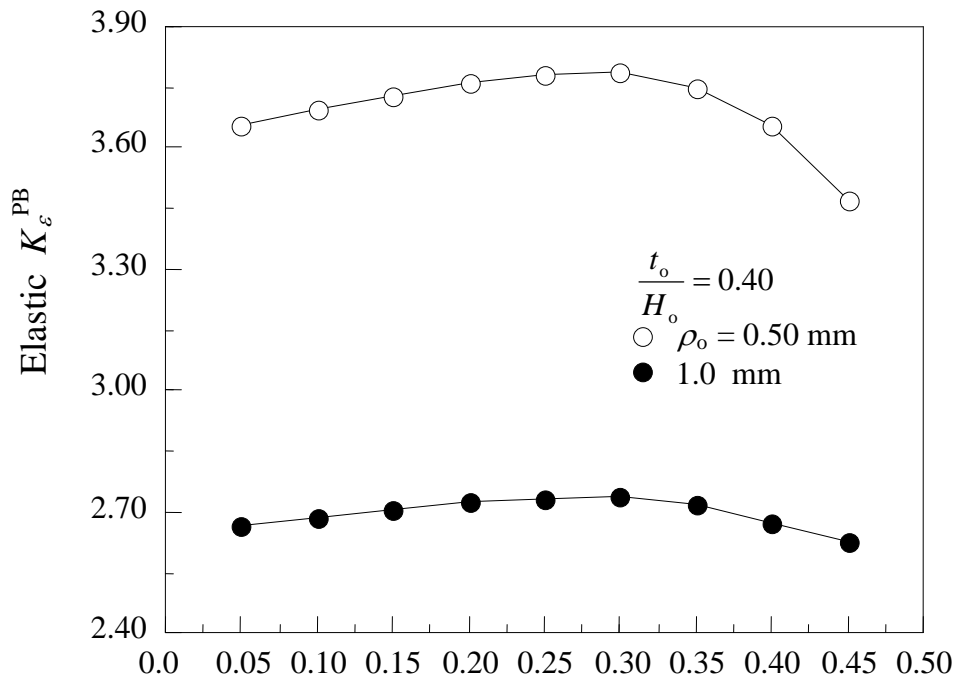


Figure 21. Variation of the elastic K_ϵ^{PB} with Poisson's ratio for $t_o/H_o = 0.40$

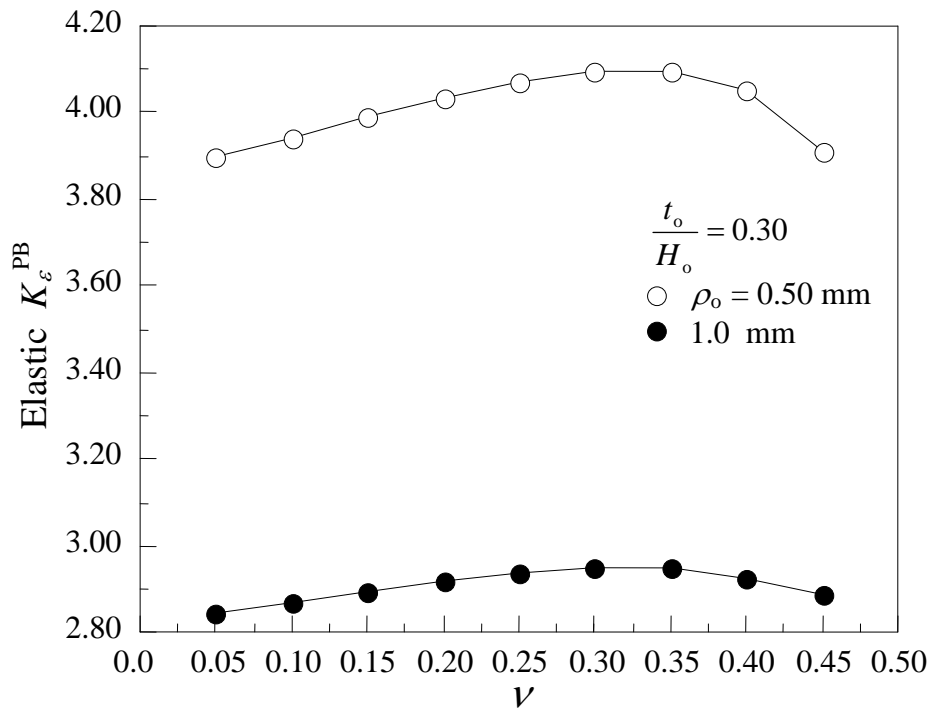


Figure 22. Variation of the elastic K_ϵ^{PB} with Poisson's ratio for $t_o/H_o = 0.30$

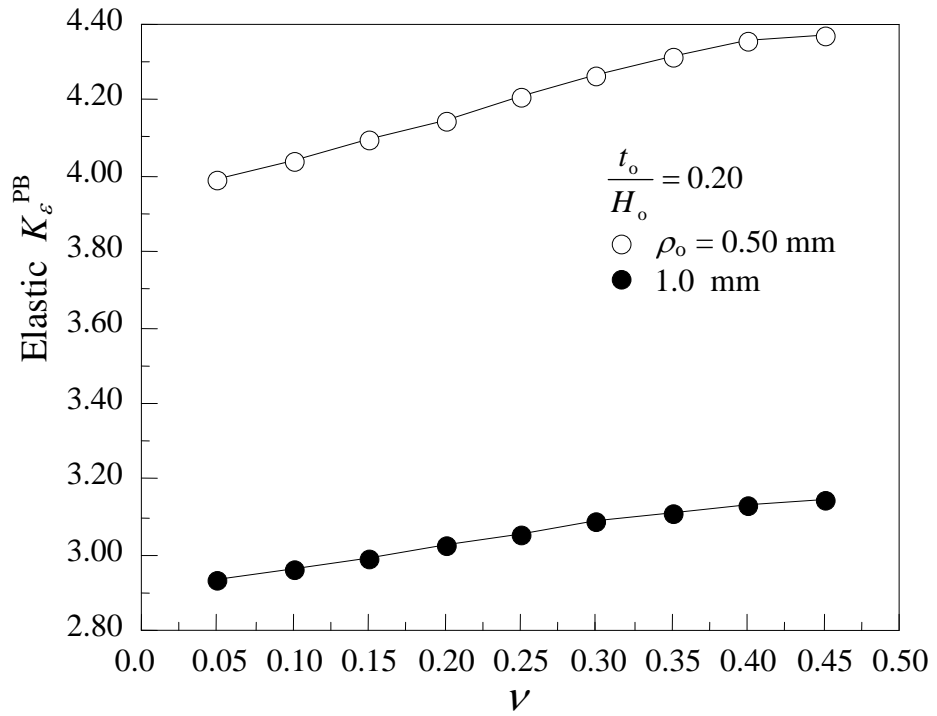


Figure 23. Variation of the elastic K_ϵ^{PB} with Poisson's ratio for $t_o/H_o = 0.20$

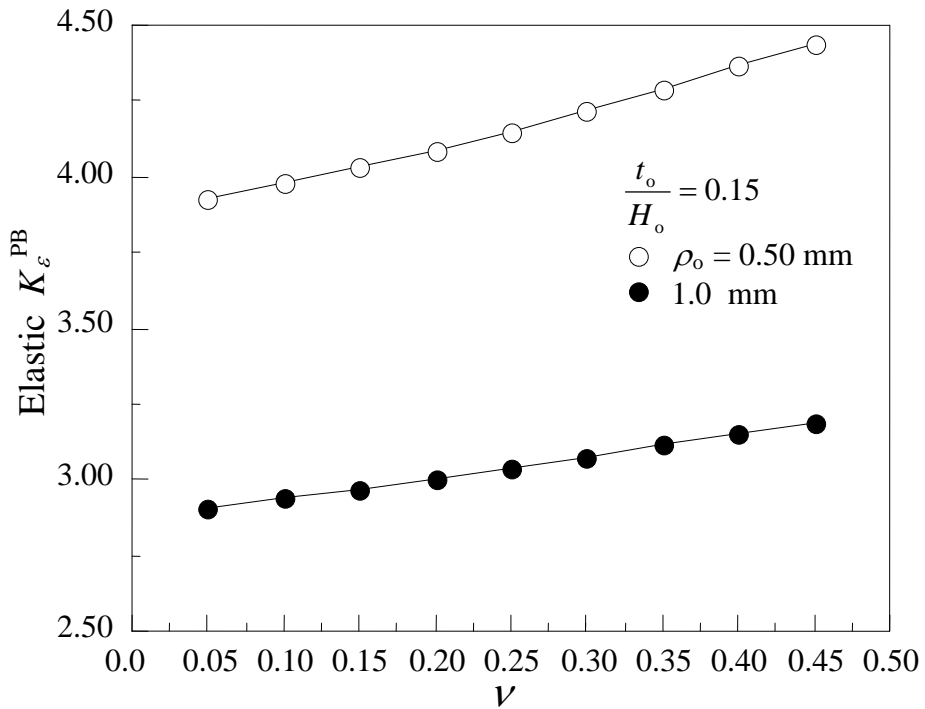


Figure 24. Variation of the elastic K_ϵ^{PB} with Poisson's ratio for $t_o/H_o = 0.15$

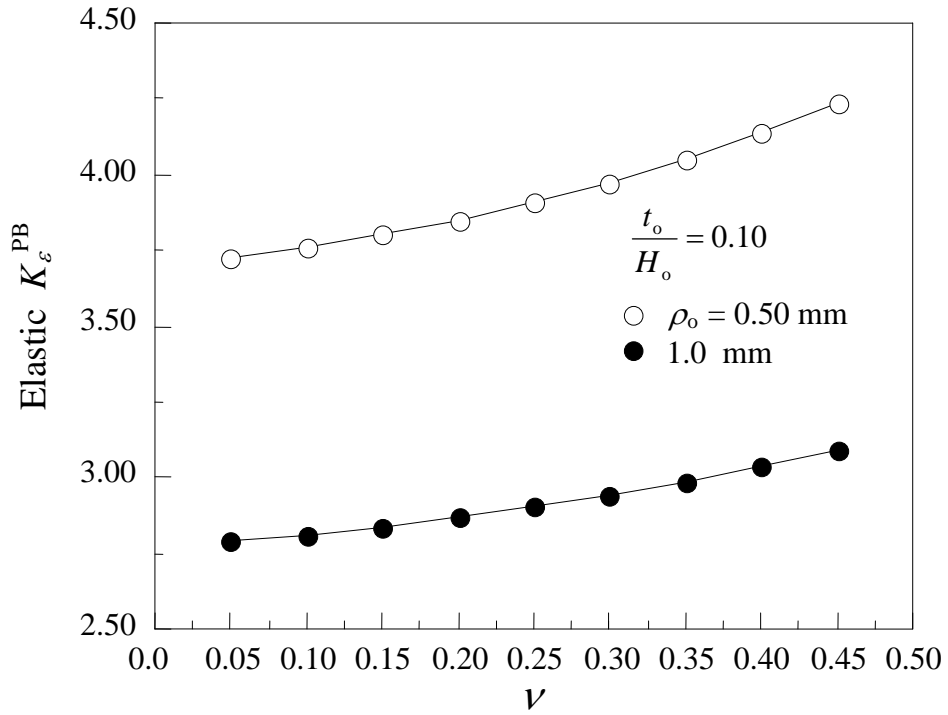


Figure 25. Variation of the elastic K_ϵ^{PB} with Poisson's ratio for $t_o/H_o = 0.10$

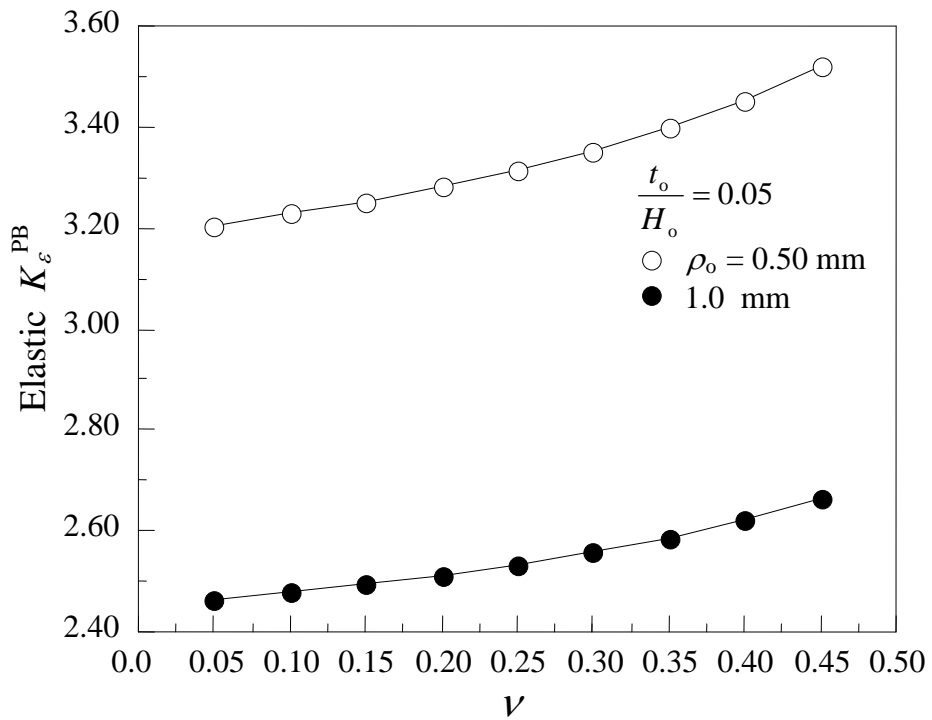


Figure 26. Variation of the elastic K_ϵ^{PB} with Poisson's ratio for $t_o/H_o = 0.05$

Table. 1. Polynomials resulting from curve fitting of the FEM results for static tension and $\rho_o = 0.50$ mm.

ρ_o [mm]	$\frac{t}{D_o}$	Equation $K_{\epsilon}^T =$
0.5	0.80	$2.303 + 0.6345 v - 1.3899 v^2 + 23.665 v^3 - 112.36 v^4 + 313.87 v^5 - 445.97 v^6 + 262.77 v^7$
	0.70	$2.748 + 0.8641 v + 1.8724 v^2 - 3.3241 v^3 + 34.302 v^4 - 90.88 v^5 + 128.69 v^6 - 48.797 v^7$
	0.60	$3.104 + 1.4191 v - 2.8240 v^2 + 44.743 v^3 - 211.89 v^4 + 620.81 v^5 - 933.28 v^6 + 603.86 v^7$
	0.50	$3.423 + 0.3905 v + 19.302 v^2 - 154.04 v^3 + 769.7 v^4 - 2072.1 v^5 + 2914.4 v^6 - 1624.4 v^7$
	0.40	$3.6097 + 1.9307 - 6.55 v^2 + 66.642 v^3 - 284.26 v^4 + 731.44 v^5 - 989.55 v^6 + 578.6 v^7$
	0.35	$3.691 + 1.6355 v - 1.7983 v^2 + 16.036 v^3 - 4.5603 v^4 - 137.21 v^5 + 398.06 v^6 - 317.54 v^7$
	0.30	$3.7024 + 3.0558 v - 30.422 v^2 + 278.71 v^3 - 1347 v^4 + 3668.7 v^5 - 5228.2 v^6 + 3047.8 v^7$
	0.25	$3.7438 + 0.8118 v + 5.8816 v^2 - 40.749 v^3 + 171.74 v^4 - 376.77 v^5 + 419.36 v^6 - 177.33 v^7$
	0.20	$3.6419 + 2.6529 v - 29.416 v^2 + 254.7 v^3 - 1209.5 v^4 + 3208.3 v^5 - 4435.3 v^6 + 2489.1 v^7$
	0.15	$3.4967 + 2.2620 v - 29.017 v^2 + 260.07 v^3 - 1301.7 v^4 + 3613.5 v^5 - 5207.3 v^6 + 3034.8 v^7$
	0.10	$3.2372 + 0.54204 v - 3.1029 v^2 + 14.464 v^3 - 49.615 v^4 + 81.029 v^5 - 51.119 v^6 - 0.25339 v^7$
	0.05	$2.7229 - 1.0816 v + 21.316 v^2 - 204.2 v^3 + 1003.4 v^4 - 2721.2 v^5 + 3823.2 v^6 - 2171.1 v^7$

Table. 2. Polynomials resulting from curve fitting of the FEM results for static tension and $\rho_o = 1.0$ mm.

ρ_o [mm]	$\frac{t}{D_o}$	Equation $K_{\epsilon}^T =$
1.0	0.80	$1.7299 + 0.5262 v - 6.0369 v^2 + 56.693 v^3 - 270.79 v^4 + 720.92 v^5 - 996.78 v^6 + 558.75 v^7$
	0.70	$2.0536 - 0.07801 v + 8.2204 v^2 - 67.199 v^3 + 332.99 v^4 - 906.09 v^5 + 1285.1 v^6 - 736.37 v^7$
	0.60	$2.297 + 0.9437 v - 6.3703 v^2 + 63.84 v^3 - 302.85 v^4 + 815.4 v^5 - 1137.6 v^6 + 647.35 v^7$
	0.50	$2.5261 + 0.5391 v + 3.5491 v^2 - 24.407 v^3 + 129.51 v^4 - 355.82 v^5 + 511.71 v^6 - 291.72 v^7$
	0.40	$2.693 + 0.9186 - 2.7365 v^2 + 35.881 v^3 - 190.41 v^4 + 573.43 v^5 - 880.16 v^6 + 546.3 v^7$
	0.35	$2.7456 + 1.1085 v - 5.6574 v^2 + 54.463 v^3 - 256.11 v^4 + 687.43 v^5 - 958.65 v^6 + 546.11 v^7$
	0.30	$2.7823 + 1.2218 v - 8.5147 v^2 + 77.625 v^3 - 368.41 v^4 + 987.75 v^5 - 1381 v^6 + 787.45 v^7$
	0.25	$2.8002 + 0.8636 v - 4.2863 v^2 + 42.374 v^3 - 216.92 v^4 + 617.76 v^5 - 904.29 v^6 + 533.34 v^7$
	0.20	$2.7716 + 0.78912 v - 5.6636 v^2 + 56.043 v^3 - 303.32 v^4 + 895.46 v^5 - 1349.2 v^6 + 812.61 v^7$
	0.15	$2.7086 - 0.54376 v + 15.579 v^2 - 139.54 v^3 + 669.2 v^4 - 1787.8 v^5 + 2491 v^6 - 1409.5 v^7$
	0.10	$2.4925 + 0.8908 v - 12.387 v^2 + 101.27 v^3 - 481.51 v^4 + 1272.6 v^5 - 1751.9 v^6 + 978.04 v^7$
	0.05	$2.1503 + 0.04384 v + 0.04198 v^2 - 11.006 v^3 + 67.815 v^4 - 213.1 v^5 + 331.52 v^6 - 202.98 v^7$

Table. 3. Polynomials resulting from curve fitting of the FEM results for pure bending and $\rho_o = 0.50$ mm.

ρ_o [mm]	$\frac{t}{H_o}$	Equation $K_{\epsilon}^{PB} =$
0.50	0.80	$2.1808 + 0.4731 v - 1.8732 v^2 + 8.3286 v^3 - 19.422 v^4 + 7.7943 v^5$
	0.70	$2.6043 + 0.4111 v + 0.0289 v^2 + 0.6716 v^3 - 8.4578 v^4 - 2.4607 v^5$
	0.60	$2.9585 + 0.9721 v - 4.8842 v^2 + 24.898 v^3 - 63.281 v^4 + 37.948 v^5$
	0.50	$3.2607 + 2.8499 v - 27.2900 v^2 + 149.6 v^3 - 374.15 v^4 + 318.87 v^5$
	0.40	$3.6145 + 0.7144v + 1.3666 v^2 - 9.5365 v^3 + 27.3440 v^4 - 54.0540 v^5$
	0.30	$3.8622 + 0.5233 v + 5.0319 v^2 - 28.972 v^3 + 80.831 v^4 - 101.85 v^5$
	0.20	$3.9553 + 0.5841 v + 4.3638 v^2 - 21.644 v^3 + 60.393 v^4 - 67.795 v^5$
	0.15	$3.8936 + 0.6563 v + 2.4926 v^2 - 9.0856 v^3 + 25.745 v^4 - 26.355 v^5$
	0.10	$3.6834 + 0.7970 v - 0.8083 v^2 + 7.2817 v^3 - 12.244 v^4 + 10.568 v^5$
0.05	$3.1814 + 0.4898 v - 0.81951 v^2 + 6.4609 v^3 - 13.182 v^4 + 12.716 v^5$	

Table. 4. Polynomials resulting from curve fitting of the FEM results for pure bending and $\rho_o = 1.0$ mm.

ρ_o [mm]	$\frac{t}{H_o}$	Equation $K_{\epsilon}^{PB} =$
1.0	0.80	$1.6891 + 0.01956 v + 1.3972 v^2 - 5.1014 v^3 + 4.0376 v^4 + 2.0317 v^5$
	0.70	$1.959 + 0.02872 v + 2.6651 v^2 - 14.388 v^3 + 28.245 v^4 - 19.385 v^5$
	0.60	$2.1794 + 1.0717 v - 9.7991 v^2 + 53.782 v^3 - 135.78 v^4 + 117.03 v^5$
	0.50	$2.4096 + 1.2559 v - 11.104 v^2 + 60.313 v^3 - 150.83 v^4 + 127.49 v^5$
	0.40	$2.6157 + 1.4347 v - 12.545 v^2 + 68.542 v^3 - 170.4 v^4 + 143.49 v^5$
	0.30	$2.8007 + 1.2122 v - 8.8776 v^2 + 48.666 v^3 - 118.13 v^4 + 94.871 v^5$
	0.20	$2.9063 + 0.6369 v - 1.2349 v^2 + 8.0993 v^3 - 16.997 v^4 + 8.4134 v^5$
	0.15	$2.8872 + 0.4217 v + 1.1411 v^2 - 3.9217 v^3 + 11.871 v^4 - 13.335 v^5$
	0.10	$2.7687 + 0.4255 v + 0.1914 v^2 + 1.4082 v^3 - 1.7842 v^4 + 2.0502 v^5$
0.05	$2.4510 + 0.2542 v + 0.17601 v^2 + 0.8397 v^3 - 1.5334 v^4 + 2.6662 v^5$	

Revision of the Recent Heterogeneous Solid Object Modeling Techniques

Wisam Abu Jadayil

Department of Industrial Engineering,

The Hashemite University,

Zarqa, Jordan 13135

Abstract

This paper discusses the most recent and common technologies for modeling heterogeneous objects composed of more than one material type. Researchers have found the great need for heterogeneous modeling of objects in order to get the required properties of the object material. Eight technologies for modeling heterogeneous objects have been explained and discussed in this review paper. The advantages and disadvantages of each method have been introduced. Two applications of heterogeneous objects were introduced, the heterogeneous turbine blades and the heterogeneous flywheel. Comparison of the most common methods of rapid prototyping has been made in the review.

It has been found that all present heterogeneous modeling technologies have many limitations. So, there it is required to develop an effective heterogeneous modeling technology that takes into consideration both the design geometry and the material composition simultaneously. Using wavelets in the mathematical representation of heterogeneous objects might greatly help in finding that perfect technology.

© 2010 Jordan Journal of Mechanical and Industrial Engineering. All rights reserved

Keywords: : Heterogeneous modeling, Wavelets, Rapid Prototyping, Composite material.

1. Introduction

The modeling and representation of heterogeneous object is an important research area that extensively published nowadays. Recently, several rapid prototyping technologies are at a point where building heterogeneous objects became more realizable. Thus, methodologies to design the 3D object computer model for free fabrication should be developed [1].

Recently, scientists and engineers have studied the manufacturing of heterogeneous objects, mainly in the form of composites. This is because of the many advantages and good properties of heterogeneous products over the homogeneous object product in many applications. But there should be a control for the heterogeneity in order to achieve the desired functionalities [1].

The recent development of heterogeneous object modeling offers new potentials of many applications. That is in heterogeneous object multiple materials are synthesized with certain proportions to provide better properties than that obtained from using any of these materials alone.

In many applications, the product object should have certain properties to be able to resolve its function, like heat resistance and anti-oxidation properties on high temperature side, mechanical toughness and strength on the low temperature side, and the effective thermal stress relaxation throughout the material. Such properties cannot be obtained by using single material or homogeneous

object, so the trend to heterogeneous object modeling is clearly noticed in the recent research [2].

On the other hand, there should be an effective design method, and effective rapid prototyping technology that allows the designer to take into consideration both the design geometry and the material composition simultaneously. In the heterogeneous object design, the properties of that object can be adjusted by controlling the material composition, microstructure and the geometry of the object. So, in order to obtain a heterogeneous object model for analysis and fabrication, an effective design method is needed.

Until recently, prototypes had to be built by model manufacturer from 2D engineering drawings. Of course this has many disadvantages, like time-consuming, high costs and the less precision in identical products. But nowadays, using CAM/CAD technologies made prototypes are rapidly produced from 3D computer model [3]. This describes how much it is important to improve these technologies.

The term for describing a process of producing accurate parts directly from CAD models in few hours, with little need for human intervention, is Rapid prototyping (RP) [3].

From the advantages of the advance of the rapid prototyping (RP), or solid free form fabrication (SSF) is that it eliminates the high cost of tooling and design changes or material substitution. This is by allowing rapid fabrication of form and fit models without the need for tooling or extensive machining. Through service bureaus, RP has become increasingly available to small businesses.

An approach for direct fabrication of components that can be used for a wide range of engineering materials is the computer-aided manufacturing [4].

The main advantage of the RP is the ability to quickly translate the computer aided design (CAD) databases into solid facsimiles of concept designs to help with production development.

Building shapes using selective material-additive processes has a far-reaching advantage; the creation of heterogeneous structure composed of multi material regions with prefabricated devices embedded into the structure. Fabrication of heterogeneous structure is so important that it enables the realization of new and complex designs. The layered manufacturing (LM) processes consist of two-step methodology. The first step is to decompose the 3D CAD model of the object into cross-sectional layers, and the second step is to use material additive processes to physically build up these layers and form the object (CAM) [5].

There are many different technologies of object modeling and rapid prototyping. Each of them has its advantages over the other technologies and has its limitations, which makes the door still opened for more research in this field.

This paper is mainly talking about the main technologies developed for object modeling. The characteristics and limitations of those technologies are described in section 2. Section 3 contains two examples of the applications of two recent technologies. And since the object modeling is the first step of object manufacturing, this paper is talking briefly, in section 4, about the rapid prototyping technologies the second and final step in the manufacturing of an object. Section 5 describes the advantages and limitations of the modeling and RP technologies, the discussion of these advantages and limitations and the need for new technology and future directions of research is in section 6. Finally, the conclusion is stated in section 7.

2. Computer Aided Design Models for Heterogeneous Objects

The following research topics clarify the development stages that the computer Aided Design models for heterogeneous objects have passed through:

2.1 Boundary Representation of Polyhedral Heterogeneous Solids

A paper of Feito and Torres in 1997 [6] presents a formal model for the boundary representation (B-Rep) of polyhedral heterogeneous solids based on a theoretical model of graphic objects. The theoretical model is the graphic object algebra, with which they managed solid modeling by enumeration, sweeping and CSG.

A formal mapping was established between the graphic objects and solid models for heterogeneous objects, which was represented by CSG and B-rep. They described the heterogeneous general polyhedron, manifold and non-manifold, with and without holes, using the algebra. Regularized operations in the algebra are the generalization of Boolean regularized operations in solid

modeling. Feito and Torres had utilized from studying of these operations to propose a B-rep method for managing graphic objects described by their boundaries. The main advantage of this is that it facilitates an abstract uniform treatment of the most important solid modeling methods.

This paper had presented a formulation of solid modeling based on the concept of graphic algebra. Feito and Torres had defined regularized operations and they proved which properties give the algebra of graphic objects a structure of vector space and Boolean algebra. This helped them so much to obtain a simple implementation. In this paper, the existence of simple objects as a generator system had been proved, which allowed them to obtain any polyhedral object starting from surplices [6].

This method presented in this paper is limited to polyhedral heterogeneous solids, which means it cannot be generalized for all heterogeneous object modeling.

2.2 Integrating the Material Information Along with the Geometry Topology in the Solid Model

Kumar and Dutta (1997) proposed a new approach for modeling and representation of heterogeneous objects. In this paper they presented an approach to model and represent heterogeneous objects by integrating the material information along with the geometry topology in the solid model. They defined new modeling operations for creating and manipulating heterogeneous models and to complement traditional modeling operations. More over, they addressed the issue of computer representation of these new models [7].

By modeling and representing heterogeneous objects, they referred to the creation of a CAD model, which contains full information about the geometry, topology and material. Which means this paper had taken into consideration both the geometry and material information?

The word 'geometry' had been used to refer to both the geometry and the topology of the object. But in this paper Kumar and Dutta focused on modeling heterogeneous objects by including the variation in composition along with the geometry in the solid model. Modeling and representing the microstructure of the heterogeneous objects is a complicated problem and is beyond the scope of this paper.

This paper produces two-step process for generating the solid model. Firstly, a valid mathematical model has to be created which precisely and fully describes the shape of the object. Then, the generated mathematical model has to be stored in the computer unambiguously with minimal loss of information.

In this paper, they developed a new modeling system for heterogeneous objects. A new mathematical model for heterogeneous objects was proposed, and a computer representation for the proposed model was developed.

Kumar and Dutta had used r-sets as the basis for representing the geometry of the heterogeneous objects, and found that \mathbf{R}^n endowed with a vector space structure, is a suitable mathematical space for defining the material composition, with each dimension representing one particular primary material. The appropriate mathematical space to model heterogeneous objects is the product space $\mathbf{T} = \mathbf{E}^3 * \mathbf{R}^n$. Specifically, the material points are restricted to lie in a subset of \mathbf{R}^n called the material space \mathbf{V} . The r_m -

object is defined as the mathematical model for representing heterogeneous objects and is termed the heterogeneous solid model. The geometry of the object is captured by r -sets and the material variation is specified in each r -set by material functions.

In the application mentioned in this paper, the heterogeneous objects have material variation in only one direction, which is across the thickness or the interface region, and the commonly used distribution (or function) for these objects, is the power law.

It can be clearly seen in this work that new model (r_m -object) for representing heterogeneous objects was proposed. But the r_m -set is not general enough to model heterogeneous objects, and hence, a heterogeneous solid model, termed as r_m -object, was defined as a set of r_m -sets $\{(P_i, B_i)\}$ which are geometrically interior disjoint and are minimal. The r_m -sets capture different regions of the objects whose material can be discrete (constant) or varying continuously.

This work came at a time when all current solid modeling techniques model physical objects by representing their geometry and topology. These methods are inadequate to handle heterogeneous objects because they do not explicitly represent the object interior. On the other hand, to include material information of an object this paper proposed solid modeling schemes for heterogeneous objects by expanding beyond geometry/topology representation (based on r -sets).

Kumar and Dutta had presented another paper in 1997 in which they proposed a solid modeling scheme for materially graded objects by extending beyond geometry and topology representation based on the r -sets, to material variation in the object. The computer representation of this model was built on the existing B-Rep scheme, which made it easy to be adapted in the solid modeling systems.

Kumar and Dutta had a third paper in 1997 that has an approach to modeling multi-material objects. In this paper new mathematical model is proposed which extends the theory of r -sets and regularized Booleans to include the material information besides the topology and the geometry. This enables the r -set classes to model objects made of a finite number of materials. To facilitate the creation and the manipulations of such models, the material based Boolean operations were defined.

It can be clearly seen that the r_m -classes and the material based Boolean operations encompasses the earlier theory of the r -sets and regularized boolean proposed in the previous papers. The main advantages of this modeling scheme are that it can be built on top of existing solid modelers.

2.3 Multi-Volume CAD Modeling for Heterogeneous Object Design and Fabrication

This is a paper for SUN Wei (2000), in which the multi-volume CAD modeling system is presented based on non-manifold topological elements. Material identifications are defined as design attributes introduced along with geometric and topological information at the design stage. According to the associated material identifications in the developed multi-volume modeling system for heterogeneous object extended Euler operation and

reasoning Boolean operations for merging and extraction are executed.

Wei see that most conventional feature-based design methods are only applicable to model homogeneous structure because the features are defined and interpreted by assuming the description of the workplace as a pre-defined fabrication processing. Further more, techniques used in most rapid prototyping systems are based on the concept of material addition. The database in STL file converted from solid CAD model only contains geometric information. Therefore, feature-based design modeling is not suitable for heterogeneous structure fabrication. And so, research on multi-material and multi-attribute CAD modeling has become a recent focus.

This paper presents the salient features of the multi-volume CAD modeling useful to construct heterogeneous design objects in non-manifold geometric space. The material information is defined as design attributes and introduced along with geometric and topological information at the design stage. Extended Euler operations are used with reasoning Boolean merging and extraction operation to manipulate the design information.

So, future work should focus on developing this approach to include the formation and construction of a hierarchical structure to link feature-based design with non-manifold geometric modeling. Application of the model to solid free-form fabrication and developing advanced control algorithm tailored for the heterogeneous-material modeling information will also need to be pursued.

2.4 Modeling and Designing Functionally Graded Material Components for Fabrication with Local Composition Control

This is a paper for Jackson et. al. (1999), it presents an approach to modeling a part's geometry, topology, and composition. Their approach is based on subdividing the solid model into sub-regions, such that each region has its associated analytic composition blending functions. The blending functions had been used to define the composition throughout the model as mixtures of the primary materials available to the Solid Free Form (SFF) machine.

This paper sees that systems used for 3D object representation are based on one of the three different classes of solid modeling methods: Decomposition Models; Constructive Solid Geometry (CSG); or Boundary Representation (B-rep). Each has its merits, but their current implementations in the CAD/CAM industry do not easily permit manufacturing parts with Local Composition Control (LCC).

In fabrication with LCC not only the data structure representing all of the relevant information for its fabrication must be established, but also solid modeling method must go one step further and represent smoothly varying compositions. To be able to do this, an FGM solid modeling method must decompose the interior of the object into simpler sub-regions, each of which references information about the composition variation over its domain. This goal had been accomplished by using FGM solid modeling method based on a representation known as the cell-tuple data structure, which had been developed in a prototype form.

In traditional cell-tuple structure, a model M is decomposed into a set of cells C with each cell c_k representing a topological feature in the model, such as a vertex, edge, face or region. To represent an FGM model within the cell-tuple structure, composition information as well as geometric information is associated with each cell. In this paper approach, they had simplified the problem by beginning with models subdivided into tetrahedral meshes, permitting the use of standard meshing algorithms to convert traditional solid models to their cell-tuple representation. However, Jackson *et. al.* see that their method of subdividing the models is not the optimum, and methods for efficiently subdivide models into optimal sub-regions remains an open issue.

This paper opens the door for future work in many possible directions in the area of FGM modeling. These include implementing a larger library of cells, proposing new design and visualization methods, and establishing efficient and logical methods for subdividing traditional B-rep models into sub-regions of graded composition.

2.5 A Computational Approach to Multi-Material Solid Free Form Design Using Simulated Annealing

A computational model using the space-filling technique was developed by Khandelwal and Kesavadas to arrive an optimum way of designing such prototypes. Simulated Annealing was successfully implemented for this problem, which has ill-behaved objective function and non-convex design space characteristics. Although the computational methodology for building such multi-material SFF parts has been demonstrated successfully in this paper, but the hardware implementation requires more research.

2.6 Multiple Material Objects: from CAD Representation to Data Format for Rapid Prototyping

The information about the materials of the objects that the CAD system is used for the design work cannot be included in the contemporary CAD systems. That the production engineer usually supplies this information at the computer aided manufacturing stage. But this arrangement is inadequate in the rapid prototyping techniques even it allows multiple material objects to be produced.

So, Chiu and Tan (2000) in this paper came to propose a scheme for representing multiple material objects in the CAD system. That is multiple material objects could be fabricated in RP machine by building the material tree of the object in the CAD system's data structure, then the information is extracted from material tree, and a modified version of the STL file format is outputting to the RP machines.

Kumar and Dutta (1998) had introduced an approach for modeling multiple material objects. Their approach incorporates the representing of the material information into the representing of the geometry and topology of the object. The object is decomposed into multiple cells such that, each cell containing one type of material.

On the other hand, Chiu and Tan (2000) had proposed an alternative representation scheme for manipulating multiple material objects. They used material tree structure to represent multiple material objects, and so there is no need to subdivide into multiple cells for storing material

information, but the material information can be obtained directly from the material tree of the material boundary surfaces together with the topological and the geometrical information.

The modified STL file is a tree structure. By grouping the facets belonging to the same material boundary together, an integer representing the material index of that material boundary is assigned to the group of the facets. The arrangement of the groups of facets in the file is according to the material tree of the object. The number of the facets contained in the modified STL is sharply increased comparing to that of the original file, because as the material boundary surfaces are added into the geometrical model, more facets are formed.

2.7 'Source-Based' Heterogeneous Solid Modeling

The 'source-based' modeling scheme for heterogeneous objects had been presented and the concept of 'grading source' is proposed in the paper of Siu and Tan (2002).

In the 'source-based' modeling scheme, the object is acting as a container that is used to keep the material composition information. The content of this container is affected only by the 'water-tap', which is termed as the grading source. Which means that the geometry of the object itself is not affected by modeling of the material grading? Hence, the modifications of the material grading such as shifting, deletion and re-assignment can be done without the rearrangement of the object geometry.

The field of grading is formed when a grading source is assigned to a reference and the Euclidean space E^3 is fully occupied by the grading source. Material grading occurs in the intersection between the object and the grading sources, and according to the material distribution function $f(d)$ three grading regions and new defining operators can be defined.

Siu and Tan (2002) believed that based on their modeling scheme; there should be a development of more complicated systems for modeling operations between the containers (heterogeneous objects). To give a larger modeling flexibility to the system, they should take into considerations a larger variety of 'grading sources' and the compromised solutions between the different grading sources after Boolean operations on the containers. Further more, a modified sliced format which supports material distribution function needs to be addressed thoroughly.

Siu and Tan came back again in 2002 to present new paper discussing the scheme for modeling the material grading and structures of heterogeneous objects. In this work they focused on discussing an enhanced heterogeneous solid modeling scheme that has the capability to incorporate structure information such as the dimensions and orientation of fiber reinforcements within the heterogeneous object. On fabrication, a contour subdivision algorithm is used to discretize the material variation in each slice of the heterogeneous object.

In Siu and Tan (2002) second paper, a modeling scheme for heterogeneous objects with structure variation in the dimensions and orientation had been described, but in this study, only 1D orientation variation had been considered.

2.8 Physics-Based Design of Heterogeneous Objects

Qian and Dutta (2003) had presented a new approach for the design of the heterogeneous objects. The modeling in this approach is physics based. By specifying the material variation constrains the designer can guide the design process in this method. Only few parameters has to be used by the designer, which have the physical meaning, to make control for material composition. The material property variation is directly conceivable to the designer during the control process.

3. Applications of the Computer Aided Design Models for Heterogeneous Objects

The following are two examples to show some of the applications of the heterogeneous objects modeling:

3.1 Design of Heterogeneous Turbine Blade

The first example had been presented by Qian and Dutta (2003). This paper presents a new approach for turbine blade design, which ties B-spline representation of a turbine blade to a physics (diffusion) process.

The mathematical formulation of the approach includes three steps: using B-spline to represent the turbine blade, using diffusion equation to generate material composition variation, using finite element method to solve the constrained diffusion equation. The implementation and example presented to validate the effectiveness of this approach for heterogeneous turbine blade design.

3.2 Heterogeneous Flywheel Modeling and Optimization

This is a paper for Huang and Fadel in 2000. They demonstrate how to apply Kumar and Dutta's modeling techniques to two different kinds of flywheels, the first one consisting of finite number of distinct materials and the other consisting of two or more primary materials with continuous volume fraction variation (gradient materials). They also developed the corresponding cell-based and basis-function-based multi-objective optimization methods. These multi-objective optimization methods can be extended to the multi-objective optimization design of other heterogeneous objects.

In the conclusion of this paper, they found that Dutta's modeling methods could be applied successfully in heterogeneous flywheel modeling.

The modeling of the flywheel had been based of the following modeling techniques proposed by Kumar and Dutta; modeling of heterogeneous objects consisting of a finite number of distinct uniform materials (HD), and modeling of heterogeneous objects consisting of two or more primary materials with continuous material variation (HC).

Dutta's modeling methods had been applied successfully in heterogeneous flywheel modeling applications. Compared with cell-based approach, the basis-function based approach gives more smooth material and stress variations and saves computational time. However the cell-

based model is more suitable for rapid prototyping fabrication than the basis-function-based model if two discrete materials are used.

4. Rapid Prototyping Techniques

4.1 Direct Photo Shaping Solid Free Form Fabrication

Ventura et. al. had presented a new multiplayer solid freeform fabrication process, 'Direct Photo Shaping' (DPS). In this technique, the visible digital light projection is used as a mask-less tool to build images on photo-curable ceramic dispersions (ceramic powders in photopolymerizable liquid monomers) by flood exposure.

Direct photo shaping is a multiplayer fabrication process developed by SRI International. This process is based on layer-by-layer photo-curing of polymerizable compositions curable by visible light.

Ventura et. al. had proposed many advantages for DPS, from these advantages:

- Since each layer is shaped by flood exposure, we will get fast build up time, and so we can cure the entire profile at once.
- Minimum number of steps that is no post-processing after the fabrication of each layer is needed.
- Low cost.
- High resolution.

4.2 Solid Free Form Fabrication by Selective Area Laser Decomposition

This is a paper developed by Jakubenas et. al. in 1998. It talks about the Selective Area Laser Decomposition (SALD) as a gas phase solid free form fabrication approach to the shaping of materials without part specific tooling. SALD uses a laser beam to create a localized heated zone on a substrate-surrounded by a reactant gas.

As indicated in this paper, SALD using multiple gas precursors presents the potential for controlling both composition and microstructure in a defined shape for a wide range of materials. However, the work presented by Jakubenas et. al. does not exhaust the potential of SALD for multiple materials deposition. So, there still are many important issues to be examined to emphasize additional capabilities of the process.

4.3 Adaptive Slicing of Heterogeneous Solid Models for Layered Manufacturing

Kumar et. al. (1999) focuses on the adaptive slicing of heterogeneous objects for fabrication using LM. It is assumed that an appropriate build direction (set to be z-direction) has been chosen.

The aim of the adaptive slicing is two folds, the Dimensional Control and the Positional Control. Dimensional control achieves user specified quality in the least build time. The user specifies the surface quality as the maximum allowably cusp height for the LM model. By using one of the following strategies the positional control ensures the validity of the LM model with respect to the nominal shape. The first strategy is the 'excess deposition', in which the LM model completely encloses the nominal solid model (i.e., cusps lie outside requiring the excess

material to be removed). In the Alternative strategy 'deficient decomposition', the LM lies completely within the nominal solid model (i.e., cusps lie inside requiring a filler material).

In this paper, they had described a procedure for adaptive slicing of heterogeneous models to achieve dimensional and positional control of the LM part. The dimensional control was achieved by taking into considerations both the geometry and the material information. The geometry means the curvature of the user specified surfaces along the build direction, whereas the material information means the material variation along the build direction.

Kumar et. al. see that layer generation for a heterogeneous object is a complicated problem and there are several choices exist which are dedicated by the positional control parameters. They had discussed the appropriate strategies for these choices in their paper, and presented an algorithm that summarizes the procedure.

In this paper, Kumar et. al. did not consider the material resolution and the material variation for generating the tool-paths. A generic procedure for tool path generation for heterogeneous layers must consider both the material resolution and the geometry resolution of the process.

4.4 A Computational Approach to Multi-Material Solid Free Form Fabrication Using Simulated Annealing

This paper is by Khandelwal and Kesavadas, it a novel concept for rapidly building SFF parts by inserting prefabricated inserts into the fabricated part. To determine an ideal placement of inserts/cores in the CAD model of the part being prototyped, an algorithm was developed using the heuristic optimization technique called Simulated Annealing.

This approach has many advantages, that it will allow designers to build multi-material prototypes using Rapid Prototyping (RP) technique. More over, by using cheaper pre-fabricates instead of costly photopolymers, the production cost of the SFFs can be reduced, and it will result in reduction in the build up time, and so efficient machine utilization.

Although the name Rapid Prototyping suggests that the process is fast, the fact is that it is still a very slow and inefficient process, as the authors say. RP is an adaptive technique where layer upon layer is built progressively until the entire part is completed. Build-up time is often not a function of the geometric complexity of the part, but that of the volume and height of the part.

The second limitation of the RP technique is that only a limited choice of materials is available. Most of the RP techniques use photosensitive polymer resins.

4.5 Solid Free Form Fabrication Using Stereolithography

Perhaps the most popular among currently available RP technologies is stereolithography. The basis of the stereolithography is the formation of polymer from a photosensitive monomer resin when it is subjected to ultraviolet light.

The purpose of the paper presented by Lange and Bhavnani (1994) is to present information on how the SSF

using stereolithography process can help reduce cost and cycle time for cast metal parts.

To fabricate a part the stereolithography process uses a layer-by-layer solidification of the resin. The cure depth depends on three factors, the laser power, beam diameter and the type of the resin used.

4.6 A Comparison of Rapid Prototyping Technologies

Pham and Gault had presented in 1998 a comprehensive comparison between the rapid prototyping technologies known up to that day. Their paper included comments on the strengths and weaknesses of these technologies.

Pham and Gault (1998) had divided the RP technologies into two main categories, that involves the addition of the material and those involves the removal of the material. Kruth (1991) had divided the material accretion technologies according to the state of the prototype material before part information. Pham and Gault to include new technologies had adapted Kruth's classification. In this classification, the material addition can be divided into three main categories, according to the state of the prototype material before part information, liquid, discrete particles and solid sheets. The liquid may be solidification of a liquid polymer, solidification of an electro-set fluid (ES) or solidification of molten material. The solidification of a liquid polymer may be point by point (SL, LTP, and BIS), layer-by-layer (SGC) or holographic surface (HIS). On the other hand, the solidification of molten material can be point by point (BPM, FDM, 3DW), or layer by layer (SDM).

When the state of material is discrete particles, it can be treated by one of two methods, fusing of particles by laser (SLS, GPD), or joining of particles with a binder (3DP, SF, TSF). And finally when the state of material is solid sheets it can be treated by bounding of sheets with adhesive (LOM), or bounding of sheets with light (SFP).

Pham and Gault (1998) had summarized the main features of the different RP systems in two tables, one for commercial technologies and the other for the technologies still being researched. They found that the most accurate is the dual-jet BPM1 machine, but the maximum part size is small. The cheapest systems are the LOM3 machine and the entry-level DM system. However, LOM3 system has a drawback that parts produced are 'tacky' and so need manual assemblage. Also the low-cost DM machine has disadvantages, that its work envelope is small and it cannot manufacture shapes as complex as those created using the material accretion technologies.

Moreover, Pham and Gault (1998) had presented a figure as a quick guide for selecting RP processes. The selection is based on many factors, the end use of the part, the part size, the accessibility of the features, whether the part is hollow or not, the accuracy of the part and its strength.

5. Selection of the CAD Modeling and the RP Technologies

Table 1 shows the main advantages and limitations of the most recent CAD modeling techniques, whereas Table 2 shows most recent RP technologies, that Pham and Gault

(1998) had compared the RP technologies up to 1998, and summarized their detailed results in tables [3].

Table 1. Comparison of the advantages and the limitations of the most recent CAD modeling technologies

<u>CAD Modeling Technique</u>	<u>Advantages</u>	<u>Limitations</u>
Boundary representation of Polyhedral Heterogeneous Solids	facilitates an abstract uniform treatment of the most important solid modeling methods	limited to polyhedral heterogeneous solids, which means it cannot be generalized for all heterogeneous object modeling
Integrating the Material Information Along with the Geometry Topology in the Solid Model	Had taken into account both the geometry and the material information	-Excludes the modeling and the representation of the microstructure -material variation in only one direction
Multi-Volume CAD Modeling for Heterogeneous Object Design and Fabrication	-multi-volume CAD modeling system is presented based on non-manifold topological elements -material information is introduced along with the geometric and topological information	-Does not include the formation and construction of a hierarchical structure -Application of the model to solid free-form fabrication and developing advanced control algorithm is needed.
Modeling and Designing Functionally graded material Components for Fabrication with Local Composition Control	presents an approach to modeling a part's geometry, topology, and composition	Method of subdividing the models is not the optimum
A Computational Approach to Multi-Material Solid Free Form Design Using Simulated Annealing	-allow designers to build multi-material prototypes -reduction of the production cost -reduction of the build up time -efficient machine utilization	-No hardware Implementation -build up time is a function of the volume and height of the part.
Multiple Material Objects: from CAD Representation to Data Format for Rapid Prototyping	-Representing multiple material objects in the CAD system -The material information can be obtained directly from the material tree	The number of the facets contained in the modified STL is sharply increased
'Source-Based' Heterogeneous Solid Modeling	-Keep the material composition information -modification of the material grading can be done without the rearrangement of the object geometry	Only 1D orientation variation had been considered.
Physics-Based Design of Heterogeneous Turbine Blade	Only few parameters has to be used, which have the physical meaning	Need to be applicable for other applications

Table 2. Comparison of the advantages and the limitations of the most recent RP technologies

<u>RP Technology</u>	<u>Advantages</u>	<u>Limitations</u>
Direct Photo Shaping Solid Free Form Fabrication	<ul style="list-style-type: none"> -Since each layer is shaped by flood exposure, we will get fast build up time, and so we can cure the entire profile at once. -Minimum number of steps that is no post-processing after the fabrication of each layer is needed. -Low cost. -High resolution. 	This process is based on layer-by-layer photo-curing of polymerizable compositions curable by visible light
SFF Fabrication by Selective Area Laser Decomposition	Controlling both composition and microstructure in a defined shape for a wide range of materials	Does not exhaust the potential of SALD for multiple material decomposition
Adaptive Slicing of Heterogeneous Solid Models for Layered Manufacturing	Both the geometry and the material information were taken into consideration	Did not consider the material resolution and the material variation for generating the tool-paths
A Computational Approach to Multi-Material Solid Free Form Fabrication Using Simulated Annealing	<ul style="list-style-type: none"> -allow designers to build multi-material prototypes -reduction of the production cost -reduction of the build up time -efficient machine utilization 	<ul style="list-style-type: none"> -No hardware Implementation -build up time is a function of the volume and height of the part.
Solid Free Form Fabrication Using Stereolithography	Reduction in the cost and the cycle time for cast metal parts	Layer-by-layer fabrication, and the cure depth depends on three factors, the laser power, beam diameter and the type of the resin used

6. Discussion

Table 1 summarizes the main advantages and limitations of the most recent CAD technologies. Of the technologies listed, it can be clearly seen that the computational approach to multi-material solid free form design using simulated annealing has more advantages than the other technologies, but it has more limitations too. Each technology has one advantage or more, and at least one limitation.

The most recent techniques are the 'source-based' heterogeneous solid modeling and the physics-based design of heterogeneous turbine blade, although both of them have new advantages over the previous techniques, but still have some limitations, in the 'source-based' heterogeneous solid modeling only 1D orientation variation had been considered, and this is a special case. The physics-based design had been applied only in the modeling of heterogeneous turbine blade, but it should be

applicable for any application, not only for specific designs.

From this table we can see that until now there is no perfect technique that has all the advantages and no limitations, which make more research, is needed.

On the other hand, Table 2 summarizes the main advantages and limitations of the most recent RP technologies. By looking at this table and tables in reference [3], we can see that also among the recent and the previous RP technologies there is no perfect technology. In spite of this, the direct photo shaping solid free form fabrication and solid free form fabrication using Stereolithography seem to be the most popular RP technologies, because of their many advantages and less limitations.

As can be clearly seen in Table 1, no perfect CAD modeling technology is produced until now. So, more

research is still needed in this field. The perfect technology should include all or most of the listed advantages and no or very little limitations.

The advantages and limitations of a modeling method make it suitable for certain applications and unsuitable for the others. And so, the nature of the engineering application itself determines which CAD model to be used. For example, to design the heterogeneous turbine blade, Qian and Dutta (2001) physics-based approach is so efficient in the design of the heterogeneous turbine blade, but may be this approach is not applicable for other objects of non-physical function. On the other hand, other good modeling approaches may not be applicable for the heterogeneous turbine blade. Or the boundary representation, the turbine blade is not polyhedral. Integrating the material information along with the geometry topology in the solid model approach works only when the material variation is only in one direction, but in the turbine blade, the material variation may be in more than one direction. For the same reason, the 'source-based' heterogeneous solid modeling cannot be applicable for the design of the heterogeneous turbine blade.

Another example is the heterogeneous flywheel modeling; here Kumar and Dutta's modeling techniques were applied successfully, but other modeling techniques may not be applied here. The physics of the flywheel is different from the physics of the turbine blade, so to apply Qian and Dutta (2001) physics-based approach, more research is needed and new problem should be solved. The computational approach to multi-material solid free form design using simulated annealing is insufficient to be applied for the flywheel that the build up time is a function of the volume and the height of the part, and since the flywheel has large volume, the build up time will be long. So, the nature of the engineering application determines the chosen modeling method, but can we have new modeling technology that is efficiently applicable for all engineering applications, this future research should look for.

The main properties that the new technology should include are to include the material information besides the geometry, representing multiple material objects in the CAD system, reduction in the build-up time and production cost, to be efficient and applied easily, consider 2D and 3D orientation variation and to take into considerations the micro-structure. So, future work should look for a new CAD modeling technology that satisfy all or most of these characteristics.

On the other hand, although solid free form fabrication using stereolithography is a popular technique, research is still needed to get new and improved RP technology that avoids the main limitations of the present technologies.

7. Conclusion

Modeling and representation of heterogeneous objects is an important research area, and since building the heterogeneous objects became more realizable using rapid prototyping technologies, then methodologies to design the 3D object computer model for free fabrication should be developed. Although many modeling approaches and

many prototyping technologies have been developed, an effective design method and effective rapid prototyping technology that take into consideration both the design geometry and the material composition simultaneously is still needed.

Future work should be directed towards new modeling approaches of the heterogeneous objects that avoid the limitations of the preset technologies and to have some new properties that make them convenient for all applications, like to be as simply applied as required by the application, and to be applicable for all engineering modeling applications. A good suggestion in that direction is to start using the wavelets in the mathematical representation of heterogeneous objects. Research should be forwarded to this direction in order to find the perfect heterogeneous object technology.

8. References

- [1] T. R. Jackson, H. Liu, N. M. Partikalakis, E. M. Sachs, M. J. Cima, "Modeling and designing functionally graded material components for fabrication with local composition control". *Material and Design*, Vol. 20, 1999, 63-75.
- [2] K. J. Jakubenas, J. M. Sanchez, H. L. Marcus, "Multiple material solid free-form fabrication by selective area laser deposition". *Materials and Design*, Vol. 19, No. 1-2, 1998, 11-18.
- [3] D. T. Pham, R. S. Gault, "A comparison of rapid prototyping technologies". *International Journal of Machine Tools and Manufacture*, Vol. 38, No. 10-11, 1998, 1257-1287.
- [4] A. E. Lange, M. Bhavnani, "Solid free form fabrication using stereolithography". *SAMPE Journal*, Vol. 30, No. 5, 1994, 46-49.
- [5] V. Kumar, P. Kulkarni, D. Dutta, "Adaptive slicing of heterogeneous solid models for layered manufacturing". *Journal of Materials Processing and Manufacturing Science*, Vol. 7, No. 3, 1999, 294-312.
- [6] F. R. Feito, J. C. Torres, "Inclusion test for general polyhedra". *Computers and Graphics*, Vol. 21, No. 1, 1997, 23-30.
- [7] V. Kumar, D. Dutta, D., "An Approach to Modeling Multi-Material Objects". *Symposium on Solid Modeling and Applications*, 1997, 336-345.
- [8] V. Kumar, D. Dutta, "Solid model creation for materially graded objects," Published in *Proceedings of Solid Freeform Fabrication Symposium*, Austin.
- [9] Kumar, V. and Dutta, D., 1997, "An approach to modeling multi-material objects". 4th *Symposium on solid modeling and application*, August 1997, 336-345.
- [10] S. Sun Wei, "Multi-volume CAD modeling for heterogeneous object design and fabrication".

- Journal of Computer Science and Technology, Vol. 15, No. 1, 2000, 27-36.
- [11] D. Khandelwal, D. T. Kesavadas, "Computational approach to multi-material solid freeform fabrication using simulated annealing". Journal of Material Processing and Manufacturing Science, Vol. 7, No. 4, 1999, 405-415.
- [12] W. K. Chiu, S. T. Tan, "Multiple material objects: From CAD representation to data format for rapid prototyping". Computer-aided design, Vol. 32, No. 12, 2000, 707-717.
- [13] V. Kumar, D. Dutta, "An approach to modeling heterogeneous objects". ASME Journal of Mechanical Design, Vol. 120, No. 4, 1998, 659-667.
- [14] Y. K. Siu, S. T. Tan, "Source-based heterogeneous solid modeling". Computer-aided design, Vol. 34, No. 1, 2002, 41-55.
- [15] Y. K. Siu, S. T. Tan, "Modeling the material grading and structures of heterogeneous objects for layered manufacturing". Computer-aided design, Vol. 34, No. 10, 2002, 705-716.
- [16] X. Qian, D. Dutta, D., "Physics-based modeling for heterogeneous objects". Journal of Mechanical Design, Vol. 125, No. 3, 2003, 416-428.
- [17] X. Qian, D. Dutta, "Design of heterogeneous turbine blade". Computer Aided Design, Vol. 35, No. 3, 2003, 319-329.
- [18] J. Huang, G. Fadel, "Heterogeneous flywheel modeling and optimization". Journal of Materials and Design, Vol. 21, No. 2, 2000. 111-125.
- [19] S. Ventura, S. Narang, D. Twait, F. Lange, P. Khandelwal, E. Cohen, "Solid freeform fabrication and design". Ceramic Engineering and Science Proceedings, Vol. 21, No. 4, 2000, 111-119.
- [20] D. Khandelwal, T. Kesavadas, "A computational approach to multi-material solid free form fabrication using simulated annealing". ASME DETC Conference, Baltimore, MD, September 2000.
- [21] Kruth, "Material in-process manufacturing by rapid prototyping techniques". CIRP Annals - Manufacturing Technology, Vol. 40, No. 2, 1991, 603-614.

Hot Water Management of DHW Storage Tank: Supply Features

N. Beithou^{a,*}, M. Abu Hilal^b

^a Department of Mechanical and Industrial Engineering, Applied Science University, Amman, Jordan.

^b Department of Mechanical Engineering, An-Najah National University, Nablus, Palestine

Abstract

The current study is directed to analyze the mixing nature of cold and hot water inside storage tank, and the corresponding effects on the total usable and delivered energy to consumers. The analyses are done for two different supply features bottom and side supply of cold water. An experimental rig consisting of hot water reservoir, cold water reservoir, water pump, flow meter, hot water storage tank (HWST), and a PC with Lab-View data acquisition system, was constructed to collect the necessary data for analyses. Four different flow rates ranging from 1.9 to 10 L/min have been taken under consideration. The results were in a good agreement with the published expectations. As it is well known, low flow rates save more energy in both bottom and side cold water supply (CWS). The comparison between the two supply features showed that the side CWS has higher amount of usable hot water than the bottom CWS at the same flow rate. Side CWS also minimizes the turbulent mixing within the HWST which by its turn supply higher energy for consumers. The bottom supply feature which is easier for assembly, has a bad effect on the total usable hot water and the total amount of energy delivered to the customers. A special mechanism to distribute the water as a uniform layer from the bottom of the tank is currently under investigations.

© 2010 Jordan Journal of Mechanical and Industrial Engineering. All rights reserved

Keywords: Water Management, Hot Water, Cold Water, Mixing Process, Storage Tanks, Usable Energy, Energy Losses..

1. Introduction

World these days is suffering from the shortage in water and energy. Hot water is a precious commodity in most homes and businesses. Companies working with the manufacturing of HWSTs are working a lot to minimize losses of energy in their designs. Many HWST features are available in markets, which may look the same in shape but differ significantly in their heat transfer and flow patterns.

Many Researches have been performed to save energy by insulation, which reduces the heat losses from the HWST and the accompanied piping system [5, 10, and 11]. Special heat exchangers were proposed by Industrial Technology to recover the energy wasted during usage. Approximately 80% to 90% of all hot water energy flows down the drain, carrying with it up to 955 kilowatt-hours (kWh) of energy [8]. In an attempt to reduce the wasted energy, Barta [5] investigated mathematically the optimal insulation thickness. To reduce the heat losses from the plumbing attachments, Jing Song et al. [11] investigated the effects of plumbing attachments on heat losses from solar domestic hot water storage tanks. In purpose to verify the estimated energy savings for hot water systems, J. Wiehagen and J.L. Sikora [4] have studied the performance comparison of residential hot water systems,

in their study a laboratory test experiment was conducted to measure the energy performance of two different types of water heaters; electric storage tank and demand (tankless) heaters for different plumbing distribution systems. Results of simulation showed an increase in overall system efficiency for the demand water heater with a parallel piping distribution system over the storage tank water heater with copper piping.

These studies have been dealing with heat losses reduction, heat recovery from wasted hot water, for maximizing the hot water usage. None of the available published researches investigated what happens inside the storage tank.

As creating new resources of water and clean energy is a hard task, efforts are directed toward conservation and managing the available resources. Actually conservation of resources can be defined as more efficient or effective use of resources [3]. The efficient or effective use of resources requires spreading wide educational programs through people of how to use effectively the available resources. It is extremely important to investigate and analyze what happens while energy and water are consumed, how and why these resources are wasted.

This study is a part of a project aimed to investigate how to use effectively the available hot water resources. The project investigates deeply the hot water temperature variations within the HWST, for different supply features of the HWST.

* Corresponding author. nabil@asu.edu.jo

2. Experimental Test Apparatus

To analyze and investigate the nature of hot water temperature changes within the HWST, data on the variation of the hot water temperature should be collected under the different variable conditions; to achieve these data an experimental rig has been constructed (Figure 1). This experimental rig consist of Hot water reservoir: even though the water in the storage tank is usually heated by

solar energy or electrical energy, heating the water by solar or electrical energy needs time, to eliminate the time required to heat the water a hot water reservoir has been used. It supplies the storage tank by constant temperature hot water about 62 °C immediately when required.

•Cold water reservoir: supplies the hot water storage tank by cold water when required; it also gives the opportunity to control the CWS temperature.

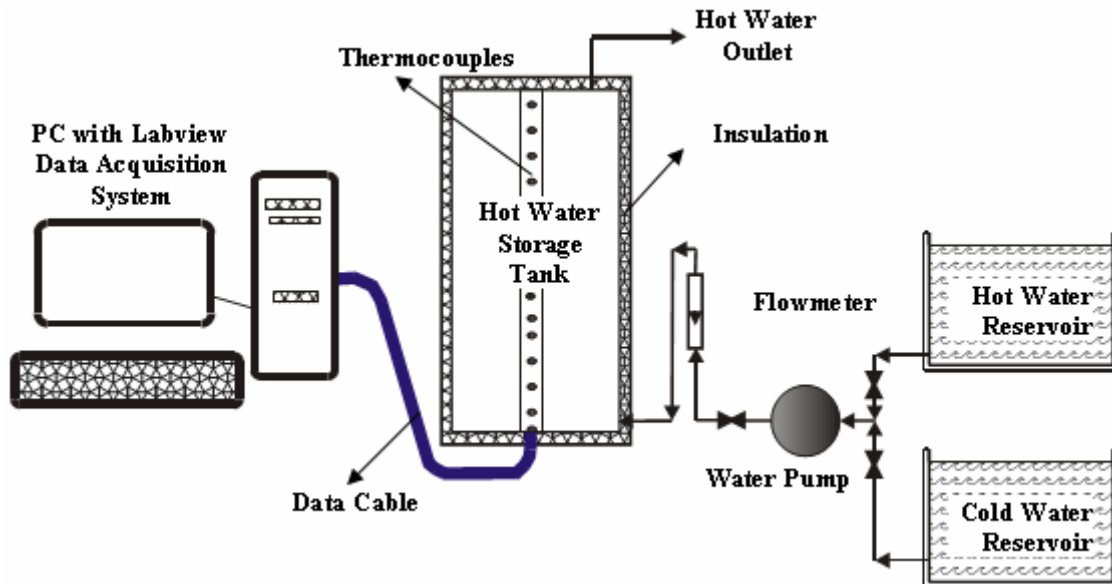


Figure 1. Schematic Diagram for the Experimental Rig

- Water pump: in order to achieve the required flow rate a water pump is used to pump hot or cold water into the storage tank, it gives the head required to overcome the losses within the piping system.
- Flow meter: Used to measure the cold water flow rate entering the hot water storage tank.
- Hot water storage tank: where hot water and cold water are mixed at the specified conditions, it is a cylindrical tank, contains a set of thermocouples to measure the temperature change within the storage tank (see table 1).

Table 1. Dimensions of the Hot Water Storage Tank.

Hot Water Storage Tank	
Height	78 cm
Internal diameter	42 cm
Number of thermocouples	15
Distance between thermocouples	5 cm
Insulation thickness	4 cm
Tank total capacity	0.108 m ³

- Data Acquisition System: (Lab-View software) consist of data cable, data acquisition card, and personal computer, it is used to collect automatically the

temperatures from the storage tank at different times and store it in a separate excel file.

In the experiments done hot water is filled into the HWST from the hot water reservoir, circulated until having a uniform temperature of 62 °C inside the tank, then the cold water from the cold water reservoir is pumped at a specific flow rate into the HWST from a side or bottom opening, the cold water is allowed to be mixed with the hot water, the temperature changes as a result of the mixing process is recorded for analyses purposes.

3. Analyses

Many hot water storage tanks are available in the markets, each has different feature as shown in figure2, some have side cold water supply others have bottom cold water supply. Manufacturers spend a lot of money to insulate the hot water tanks to minimize the heat losses, which is of a great importance in energy conservation. Nevertheless they give less attention to what happen inside the hot water storage tank during usage. The mixing nature and heat transfer mechanism associated with the different used flow rates affects the available amount of hot water to a large extend. In this work attention had been given to understand the variation of temperature for bottom and side flow CWS within the HWST, four different continuous flow rates were used from 1.9 to 10 L/min.

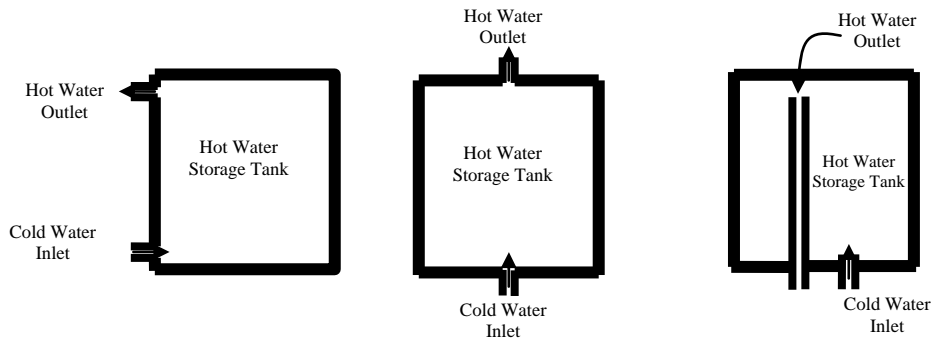


Figure 2. Features of Hot Water Storage Tanks in Markets.

For side supply of cold water, four different flow rates were used 1.9, 3.5, 5.4, and 10 L/min. Figure 3. shows the side supply cooling curves for 15 thermocouples located vertically inside the HWST (see figure1), for cold water flow rate of 1.9 L/min, the total time consumed to fill the tank with its 108 liters was 3410 sec, to cool down all thermocouples to the cold water inlet temperature it took

about 5200 sec due to heat transfer between the cold water and hot water in their mixing process. A non-uniform behavior is observed in the temperature of thermocouples 1 and 2 as a result of the turbulent mixing at the relative levels, this turbulent mixing dominates the mixing heat transfer at this region. Almost all of the other thermocouples are cooled in a uniform way, as the convection heat transfer dominates in the relative region.

Cooling Curves for Cold Water Flow Rate 1.9 L/min

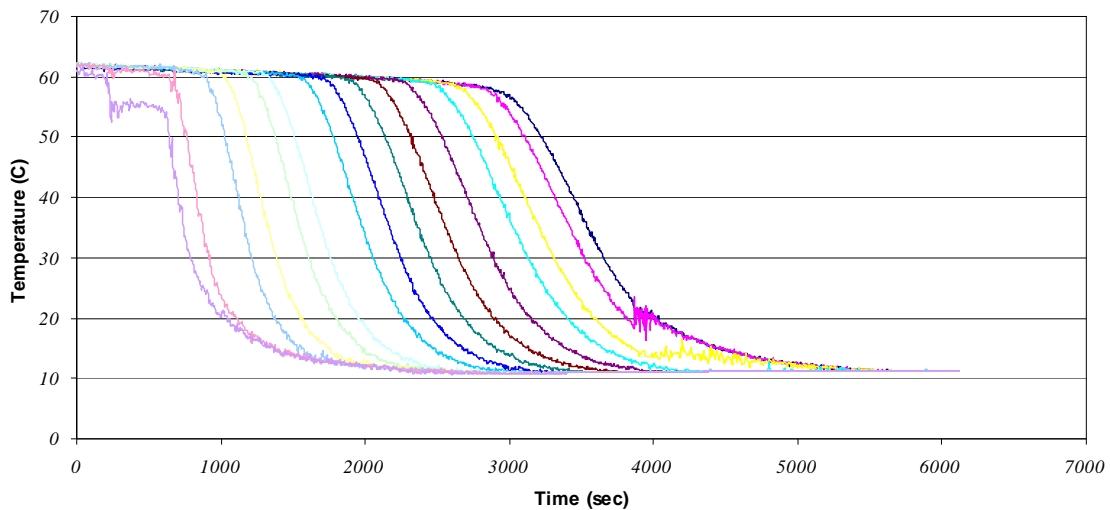


Figure 3 Cooling Curves For Cold Water Flow Rate of 1.9 L/min (side supply).

Figure 4 shows the side supply cooling curves for a cold water flow rate of 10 L/min. It is clear that a large turbulent region and non-uniform cooling curves are existed as a result of the high flow rate entering the HWST. As observed almost all of the cooling curves include a notable oscillation in temperature, this indicates the higher motion of the cold water inside the tank through the mixing process. Also it indicates that at higher flow rates a non-uniform temperature may be obtained from the HWST.

For bottom supply of cold water, again four different flow rates were taken; these are 3, 6, 8, and 9 L/min. Figure 5 shows the cooling curves within the HWST for cold water flow rate of 3 L/min, as it can be observed from figure 5 the first three thermocouples were cooled together, which means that the corresponding flow rate 3 L/min had made a turbulent flow within the first 15 cm of

the HWST. The rest of the thermocouples were cooled in a uniform way. Small oscillations were observed in the temperature at the different levels within the tank, this shows that there is a simple turbulence in the flow within the tank. Figure 6 show the cooling curves within the HWST for cold water flow rate of 9 L/min. It is clear that turbulent mixing is dominant, and almost all the tank gets to have the same low temperature after a short period of time. This means that a short amount of hot water can be used in such a case and the rest of the hot water comes to be with a low temperature which can not be used as hot water.

In general, the heat transfer mechanisms within the entire tank can be divided into two parts, one of which depends on the direct contact between the hot and cold water, and heat then is transferred as a result of convection, the other is resulted from the high flow rate in

Cooling Curves For Cold Water Flow Rate Of 10 L/min

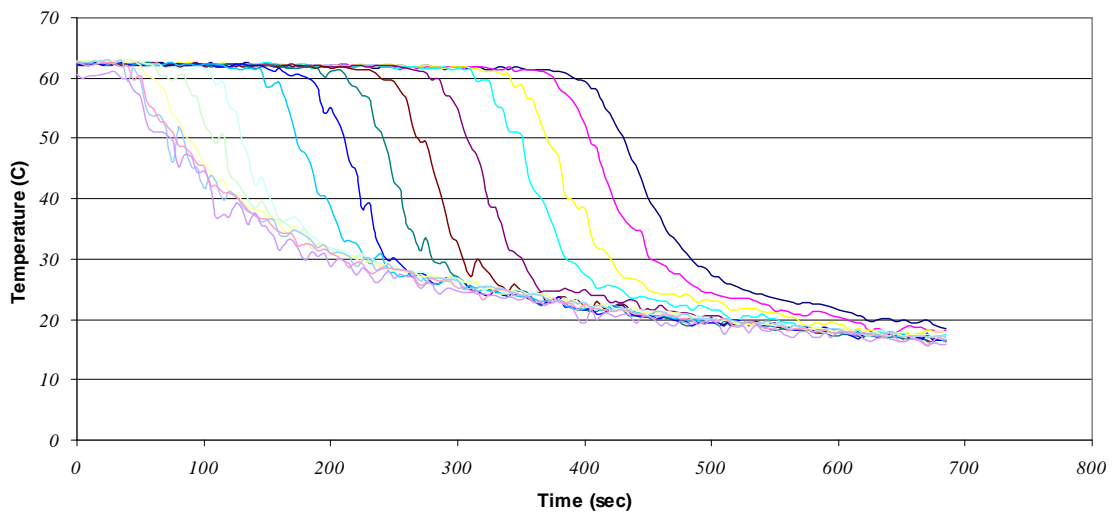


Figure 4 Cooling Curves For Cold Water Flow Rate of 10 L/min (side supply).

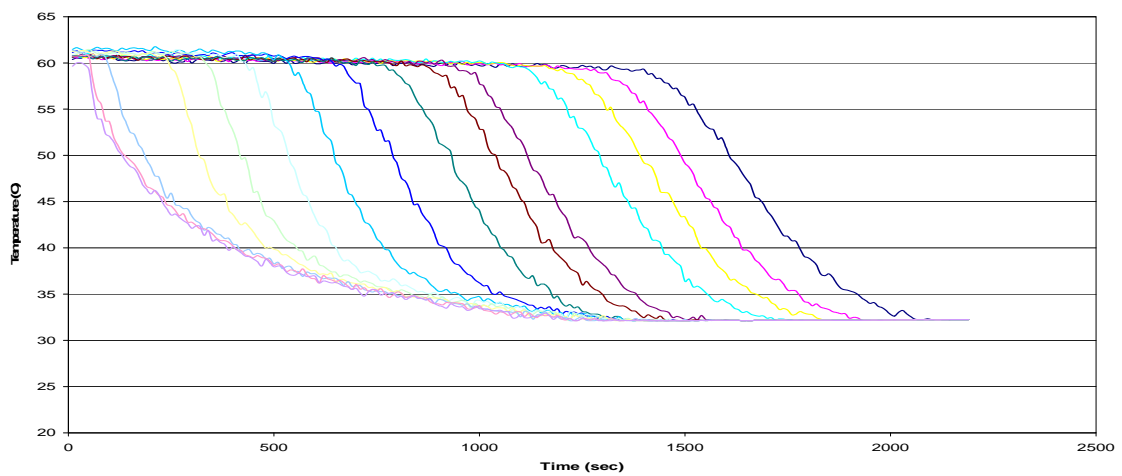


Figure 5 Cooling Curves For Cold Water Flow Rate of 3 L/min (bottom supply).

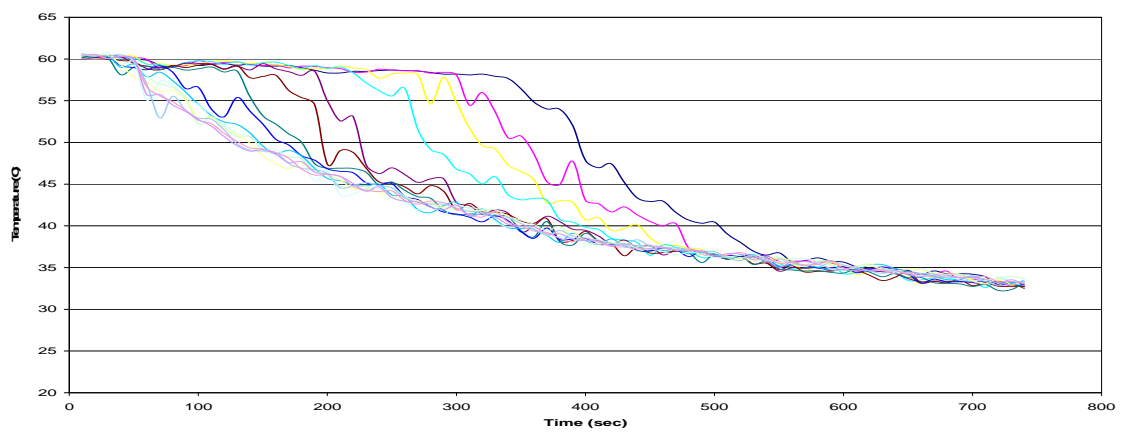


Figure 6 Cooling Curves For Cold Water Flow Rate of 9 L/min (bottom supply).

the relative levels within the tank, this create turbulent mixing of the cold and hot water inside the tank which by its turn accelerates the heat transfer between the cold and hot water layers, and drop significantly the temperature of the hot water that is supplied to consumers.

The total usable hot water available versus the cold water flow rate was drawn for both cases of bottom and side CWS features as indicated by figure 7. It has been observed that in the side CWS and for the flow rates between 1.9 to 10 L/min, a range between 110 to 75 L/min were achieved, where as for the bottom CWS feature and for a cold water flow rates between 3 to 9 L/min, a range between 90 to 55 L/min were achieved. The large drop in the amount of usable hot water is related to the high

turbulent mixing in the case of bottom CWS. Thus the use of bottom CWS in the HWST waste a large amount of the usable hot water as a result of turbulent mixing.

In figure 8, the total delivered energy to the customer was analyzed for both features. It has been found that the energy supplied to the customers ranges from 27000kJ to 19000 kJ, in the side CWS. Whereas, total delivered energy ranges from 21000 kJ to 15000 kJ in the bottom CWS. This result indicates that bottom supply of cold water does not only reduce the amount of the usable hot water, but also reduces the total energy supplied to the consumers, keeping most of the collected energy within the HWST unsuitable for use.

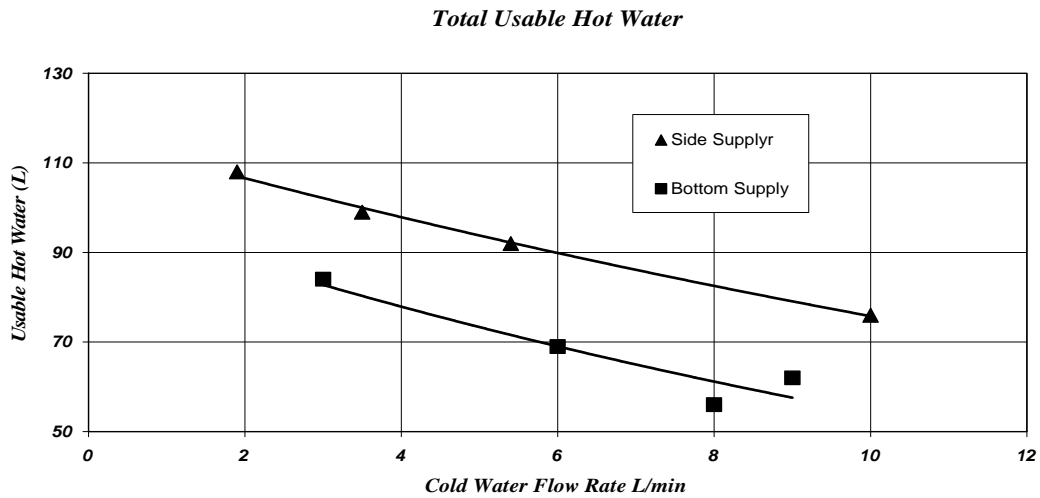


Figure 7 Total Usable Hot Water versus Cold Water Flow Rate for Bottom and Side Supply of Cold Water.

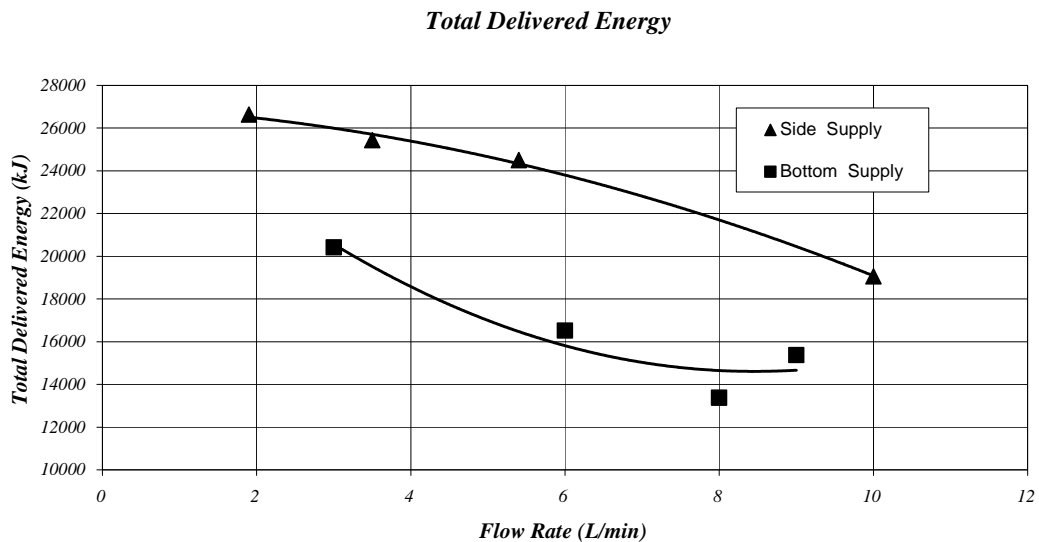


Figure 8 Total Delivered Energy For Bottom and Side Cold Water Supply.

Furthermore, the time required to cool each thermocouple (node as shown in Figure 1) in the HWST was drawn in figure 9. It has been found that for small flow rates the time needed to cool the nodes increases by going from bottom to top of the HWST, whereas, for high flow rates less time was required (as expected [14]).

Figure 9, indicates that for low flow rates the

convection heat transfer is dominant and thus more time will be required to cool the higher levels as the temperature of the higher nodes gets closer to each other thus minimizes the heat transfer rate. At the higher flow rates turbulent mixing heat transfer will dominate which by its turn will reduce the time required to cool the different thermocouple within the HWST.

Time Required to Cool Nodes From 57 C to 42 C

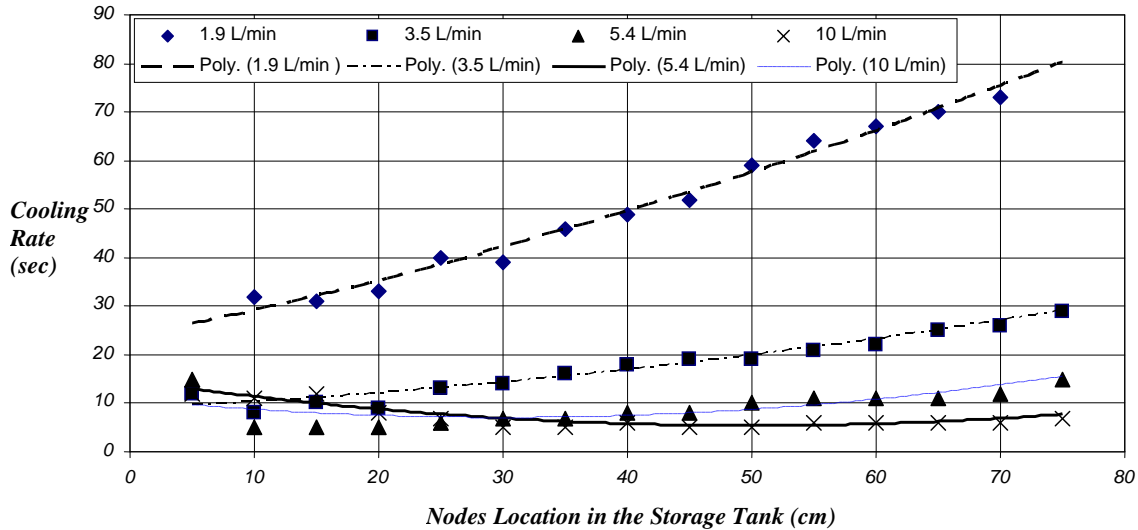


Figure 9 Time Required for Cooling Nodes From 57 °C to 42 °C.

4. Conclusion

Energy conservation is defined as more efficient or effective use of energy. As fossil fuel costs rise and environmental concerns grow, more efficient energy conservation and utilization technologies become cost effective. However, technologies alone can not produce sufficient results without continuing management efforts. This study is directed toward analyzing the heat transfer between the cold and hot water inside the storage tank for both bottom and side CWS features. Experiments Results show that low flow rates save more energy for consumption in both cases. The comparison between the two supply features suggests the use of side CWS which gives higher amount of usable hot water than bottom CWS at the same flow rates. Side CWS also minimize the turbulent mixing within the HWST which by its turn supply higher energy for consumers. For small flow rates convection heat transfer is the dominant mechanism where the turbulent mixing heat transfer dominates at high flow rates. It is clear that the bottom supply feature has a bad effect on the total usable hot water, and there is a need to stop the turbulent mixing in the HWST. A special mechanism to distribute the water as a horizontal uniform layer from the bottom of the tank is currently under investigations.

References

- [1] N. Beithou, "Heat Transfer Aspects in Bottom Flow Mixing of Cold Water and Hot Water in Domestic Hot Water Storage Tank", Accepted for publication Journal of Mechanical Engineering, 2006.
- [2] Sezai, L. B. Y. Aldabbagh, U. Atikol, H. Hacisevki "Performance Improvement by using Dual Heaters in a Storage-type Domestic Electrical Water-Heater", Applied Energy, Vol. 81, pp. 291-305, 2005.
- [3] N. Beithou, "Proposed Water Management and Control Device for Water Losses Problem in Jordan" Accepted for publication, JEES, 2005.
- [4] Wiehagen J., Sikora J.L., "Performance Comparison of Residential Hot Water Systems" NAHB Research Center, Upper Marlboro, Maryland, NREL/2003.
- [5] Barta L., "Energy Conservation of Domestic Hot Water Distribution Systems", 27th International Symposium CIB W62 Water Supply and Drainage for Buildings, September 17-20, 2001, Portoroz, Slovenia.
- [6] Takata H., Murakawa S., Nishina D., and Koshikawa Y., "An Analysis on the Load of Hot Water Consumption in the Apartment Houses", 27th International Symposium CIB W62 Water Supply and Drainage for Buildings, September 17-20, 2001, Portoroz, Slovenia.
- [7] Merrigan, T., "Residential Conservation Demonstration Program: Domestic Hot Water", Florida Solar Energy Center, Cape Canaveral (USA), Technical Report, 2001 May 13.
- [8] Industrial Technologies, "Waste Fluid Energy Recovery System Recycles Waste Energy and Cuts Utility Bills",

- Office of Industrial Technologies, Energy Efficiency and Renewable Energy, US Department of Energy, June 2000.
- [9] Calmeyer JE., Delpont GJ., " Hot water Load Control Within Communal Living Environments Such as Residences and Hostels", Domestic Use of Electrical Energy Conference, Cape Peninsula University of Technology, Cape Town South Africa, 1999.
- [10] Forlee C., " A flexible Hot Water Load Control System", Domestic Use of Electrical Energy Conference, Cape Peninsula University of Technology, Cape Town South Africa, 1999.
- [11] Jing Song, Liang-Jun Ji, Byard D. Wood," Effects of Plumbing Attachments on Heat Losses from Solar Domestic Hot Water Storage Tanks" NREL, March 1998.
- [12] Burch J., Xie Y., Murley C. S.," Field Monitoring of Solar Domestic Hot Water Systems Based on Simple Tank Temperature Measurement" , NREL, May 1995.
- [13] Papakostas, K.T. ; Papageorgiou, N.E. ; Sotiropoulos, B.A," Residential Hot Water Use Patterns in Greece", Solar Energy ; VOL. 54 ; ISSUE: 6 ; PBD: Jun 1995, pp. 369-374 ; PL
- [14] ASHRAE Handbook," Heating Ventilation and Air Conditioning Applications", ASHRAE, Inc., 1995.



الجامعة الهاشمية



المملكة الأردنية الهاشمية

المجلة الأردنية
للمهندسة الميكانيكية والصناعية

JJMIE

مجلة علمية عالمية محكمة

<http://jjmie.hu.edu.jo/>

ISSN 1995-6665

المجلة الأردنية للهندسة الميكانيكية والصناعية

مجلة علمية عالمية محكمة

المجلة الأردنية للهندسة الميكانيكية والصناعية: مجلة علمية عالمية محكمة تصدر عن عمادة البحث العلمي والدراسات العليا في الجامعة الهاشمية بالتعاون مع صندوق دعم البحث العلمي في الأردن.

هيئة التحرير

رئيس التحرير:

الأستاذ الدكتور موسى محسن
قسم الهندسة الميكانيكية، الجامعة الهاشمية، الزرقاء، الأردن .

الأعضاء:

الأستاذ الدكتور عدنان الكيلاني الجامعة الأردنية	الأستاذ الدكتور بلال العكش الجامعة الهاشمية
الأستاذ الدكتور أيمن المعاينة جامعة مؤتة	الأستاذ الدكتور علي بدران الجامعة الأردنية
الأستاذ الدكتور محمد النمر جامعة العلوم والتكنولوجيا الأردنية	الأستاذ الدكتور نسيم سواقد جامعة مؤتة

مساعد رئيس هيئة التحرير:

الدكتور أحمد الغندور
الجامعة الهاشمية

فريق الدعم:

<u>تنفيذ وإخراج</u> م. أسامة الشريط	<u>المحرر اللغوي</u> الدكتور عبدالله جرادات
--	--

ترسل البحوث إلى العنوان التالي :

ترسل البحوث إلى العنوان التالي:
رئيس تحرير المجلة الأردنية للهندسة الميكانيكية والصناعية
عمادة البحث العلمي والدراسات العليا
الجامعة الهاشمية
الزرقاء - الأردن

هاتف : 00962 5 3903333 فرعي 4147

Email: jjmie@hu.edu.jo

Website: www.jjmie.hu.edu.jo